Iranian Journal of Fuzzy Systems

Volume 22, Number 5, (2025), pp. 69-96

Original paper

Evolutionary fuzzy control of pandemics with vaccination and isolation constraints

H. Rafiei[1], A. Salehi[2], F. Baghbani[3] and M. R. Akbarzadeh-T.[4]

[1,2,4]*Department of Electrical Engineering, Center of Excellence on Soft Computing and Intelligent Information Processing, Ferdowsi University of Mashhad, Mashhad, Iran*

[3]*Department of Electrical and Computer Engineering, Semnan University, Semnan, Iran*

rafiei.hamed@mail.um.ac.ir, alisalehi@mail.um.ac.ir, baghbani.fahimeh@semnan.ac.ir, akbazar@um.ac.ir

Abstract

Vaccination and isolation are crucial strategies for controlling pandemics, but healthcare infrastructure constraints, such as limited medical resources and workforce shortages, often limit their effectiveness. This research explores the impact of these constraints on vaccination and isolation policies through the development of a Vaccination and Isolation Constraint-based Evolutionary Type-2 Fuzzy Controller (VIETFC) intended to assist policymakers. A genetic algorithm optimizes VIETFC's parameters to reduce the number of infected individuals and provide adequate medical care. As a realistic case study, we consider the COVID-19 pandemic and use a stochastic SEIAR (S^2EIAR) model to include the pandemic's inherent uncertainties and establish four scenarios with progressively increasing constraints, with the fourth scenario reflecting the most realistic conditions. Results show that VIETFC adapts effectively to resource limitations, maintaining a 15% standard deviation despite a 50% parameter variation. VIETFC surpasses Proportional Integral Derivative (PID) and type-1 fuzzy controllers by offering interpretable solutions through a more practical resource allocation strategy. Future research should focus on enhancing the flexibility of this method for application to additional pandemic models.

Keywords: Pandemics, type-2 fuzzy control, vaccination rate, isolation rate, genetic algorithms.

1 Introduction

The recent COVID-19 outbreak raised awareness on the fragility of modern life against pandemics and its wide-scale economic and public health impact. Since its emergence in 2019, numerous studies have focused on this virus's mathematical modeling and pandemic control to improve our understanding and enhance our ability to manage the virus or similar outbreaks effectively. Some works introduce innovative mathematical dynamics, while others focus on developing controllers using these dynamics. However, uncertainties impede the performance of models and controllers that rely on precise information. Hence, intelligent paradigms that could effectively represent or manage these uncertainties, such as in fuzzy logic and probabilities, could lead to realistic mathematical models that reflect real-world pandemic dynamics.

In 2022, Mehra et. al. [27] developed a Susceptible Exposed Infected Asymptomatic Recovered (SEIAR) model and investigated its basic reproduction number and the equilibrium points using the Influenza Epidemic Model. Unlike Susceptible Exposed Infectious Recovered (SEIR) models, the SEIAR model considers the possibility of transmission from asymptomatic to the infected population (symptomatic and infectious). Additionally, it incorporates birth and natural death rates into the model. The authors then employed SEIAR for COVID-19 control using vaccination and isolation strategies [1].

Corresponding Author: M. R. Akbarzadeh-T.

Received: November 2024; Revised: August 2025; Accepted: September 2025.

https://doi.org/10.22111/ijfs.2025.50369.8889

In our previous study [38], we enhanced SEIAR to a stochastic SEIAR (S^2EIAR) model and incorporated uncertain parameters and variables to capture real-world pandemic dynamics better. The S^2EIAR was then utilized to manage the pandemic through type-2 fuzzy systems. The type-2 fuzzy systems, as knowledge-based systems with capabilities for approximation and uncertainty management, are valuable tools for tackling decision-making challenges associated with the pandemic. However, reaching the optimal parameter settings for a type-2 fuzzy system is nontrivial, and much of it is often considered metaknowledge. Hence, a genetically optimized type-2 fuzzy controller was suggested to determine vaccination and isolation strategies to follow the desired infection rate curve. Specifically, two scenarios were examined, with the infection rate following two predetermined fixed and Gaussian curves. However, the previous work did not account for the limitations imposed by the real world on isolation and vaccination capacities, as there are consistently restricted resources and infrastructure for these policies.

The current study develops a new type-2 fuzzy control system for controlling COVID-19 that considers these limitations and explores various realistic scenarios. Similar to [38], type-2 fuzzy systems are utilized as the control system due to their expanded ability and added degrees of freedom in uncertainty representation, hence outperforming their type-1 counterparts, especially when dealing with uncertainties related to language, rules, or data [28]. This paradigm can be an excellent candidate for controlling COVID-19 spread and allocating proper resources affecting vaccination and isolation policies against pandemic uncertainties. In contrast to our previous work [38], which assumed no resource limitations on control inputs, the type-2 fuzzy controller establishes vaccination and isolation rates based on their upper constraints and the number of infected individuals. We optimize key parameters of the fuzzy controller, including the membership functions and the number of fuzzy rules, through genetic algorithms. This design process is applied to four realistic scenarios featuring both constant and time-varying constraints on vaccination and isolation capacities. This proposed strategy, we hope, marks a significant advancement over our earlier study [38], which only examined two simpler scenarios without real-world resource limitations.

In short, the main contributions of this paper are summarized below:

- The proposed method includes the limitations on both vaccination and isolation strategies directly in the control design via an appropriate fuzzy system. This stands in contrast to the works such as [24]-[32] that primarily focus on vaccination limitation and apply it to the generated control signal in an optimal control strategy. Specifically, the proposed type-2 fuzzy system, optimized by a genetic algorithm, determines the vaccination and isolation rates based on the previous day's upper bounds and the number of infected individuals.
- The current approach differs from our earlier work [38] by establishing the upper bounds for vaccination and isolation rates based on their upper bounds imposed by the infrastructure constraints and the number of infected individuals. The current study also optimizes the number of fuzzy rules using genetic algorithms and considers four realistic scenarios involving resource and supply constraints, aspects that were overlooked in [38].
- Real-world scenarios of time-varying upper bounds and limited supplies are introduced to evaluate the control performance. Our approach is based on the availability of resources rather than the minimization of the vaccination/isolation cases often found in optimal control strategies (e.g., [19]).
- The proposed work is evaluated under four scenarios, considering both vaccination and isolation limitations, rather than focusing solely on vaccination administration limitations, as seen in [32].

The remainder of the paper is organized as follows: Section 2 reviews some recent works on modeling and control of COVID-19. Section 3 defines the S^2EIAR model. Section 4 introduces the proposed VIETFC and formulates the genetic algorithm problem. Section 5 introduces the scenarios and results. Section 6 provides the discussion. Finally, conclusions are stated in Section 7. Furthermore, ablation studies on PID and type-1 fuzzy controllers are provided in the Appendix.

2 Related works

This section provides an overview of the literature on COVID-19 modeling and control. We begin by exploring various mathematical models employed in COVID-19 research, both deterministic and enhanced stochastic models. Next, we analyze the strategies used to control COVID-19, which are primarily centered around vaccination and isolation efforts. We first explore control strategies that do not account for real-world constraints, and then we review studies that incorporate these limitations into their control designs.

Most studies focus on deterministic models that consider different parameters mainly based on the number of Suspected, Infected, and Recovered (SIR) cases as presented in [3] along with more complex models that include

Nomenclature

Symbol	Definition	Symbol	Definition
S	Susceptible population	A	Asymptomaticpopulation
E	Exposed population	R	Recovered population
I	Infected population	N	Total population
β	Susceptible population rate	κ	Infection rate of exposed population
ε	Infectivity reduction of exposed population	z	Recover fraction of asymptotic population
q	Contact reduction by isolation	η	Recover rate of asymptotic population
δ	Asymptomatic population's infectivity reduction	α	Recover rate of infected population
ρ	Infection fraction of exposed population	f	Recover fraction of infected population
$\underline{x}$	Model variables' vector	$\underline{\pi}$	Model parameters' vector
u_{Is}	Isolation rate of infected population	u_{Va}	Vaccination rate of suspected population
$\overline{U}_{Va}$	Vaccination rate upper limit of suspected population	$\overline{U}_{Is}$	Isolation rate upper limit of infected population
$\tilde{}$	Over a model parameter or variable indicates uncertainty	υ	Fuzzy system output (vaccination fraction)
i	Fuzzy system output (isolation fraction)	u	The input vector to the fuzzy system
$\mathfrak{N}$	Additive perturbation constant of the model variable	$\mathfrak{M}$	Additive perturbation constant of model parameter
$\underline{n}$	Vector with elements belonging to $\mathcal{N}(0,1)$	$\underline{m}$	Vector with elements belonging to $\mathcal{N}(0,1)$
$\mathcal{N}(0,1)$	Normal distribution with mean 0 and variance 1		

additional population groups such as the number of dead, vaccinated, and quarantined. The studies [10, 48] also consider the exposed population and propose a Susceptible Exposed Infected Removed (SEIR) model for COVID-19 dynamics. In [30], a deterministic Susceptible-Infected-Recovered-disease induced Death-Susceptible (SIR/DS) is proposed and validated on empirical daily data of the Basque Country. Fractional order modeling of COVID-19 is also studied [22] to capture disease dynamics and memory effects in transmission. A Susceptible-Asymptotic infected-symptotic Infected-Recovered (SAIR) model is proposed for COVID-19 in [33]. A more recent study in [45] includes eight individual classes of Immature Susceptible, Susceptible, Quarantine, Awareness, Exposed, Infective, Hospitality, and Recovered to a new COVID-19 (S_iSAQEIHR) model. A Long Short-Term Memory-based recurrent neural network (LSTM-RNN) model then predicts the dynamics of COVID-19. Finally, the study [12] incorporates deep neural networks for predicting the parameters of a COVID-19 mathematical model.

Some studies also incorporate stochastic elements and uncertainties, enhancing the realism of these models by adding stochasticity to the variables (infected, recovered, and others). Specifically, the works [20, 31] consider stochastic variables in their model to address real-world uncertainties. Some studies consider uncertain parameters for their model. For instance, the uncertain parameters are addressed for a Suspected Infected Dead Recovered (SIDR) model in [26], and a SEIR model in [17]. However, a more realistic model should consider both variable and parameter uncertainties. In a previous work [38], authors proposed a stochastic Susceptible Exposed Infected Asymptomatic Recovered (S^2EIAR) model that considers both parameter and variable uncertainties by adding a random number around their mean value. More recently, a stochastic Susceptible-Asymptomatic-Infected-Removed (SAIR) epidemic model is suggested [50] to study COVID-19's dynamics and reach a stable control using the Lyapunov method.

Along with the above studies on COVID-19 modeling, some works have focused on designing control strategies. Different classic control strategies are designed for controlling COVID-19 spread, such as optimal control [8, 44], robust control [18], sliding mode control [11], adaptive control [9], Proportional Integral Derivative (PID) control [35], and predictive control [43]. Intelligent control strategies have also been proposed in some studies. For example, in [5], an LSTM network approximates the parameters of the COVID-19 model, and a sliding mode controller is used to control the disease spread. In [7], a fuzzy controller stabilizes the fractional-order chaotic model of COVID-19. Finally, predictive control systems in [25] are constructed for controlling COVID-19 based on fuzzy and wavelet neural networks.

Two main ways of controlling COVID-19 spread are isolation and vaccination [2, 49]. Accordingly, some studies have analyzed the effect of these two strategies on COVID-19 spread and included them in simulation-based control strategies. The isolation effect has been analyzed in some works [16, 39], and it is shown to be a better control strategy than lockdown [23]. Optimal control is a well-established method that seeks to minimize a cost function to achieve desired control objectives [34]. Consequently, several traditional optimal control strategies have been applied to manage the spread of COVID-19 effectively. Some optimal strategies include selecting the optimal vaccination level [15] for different COVID-19 phases. Also, based on the optimal control strategy, two scenarios are designed in [13] to minimize the number of infected individuals, viral individuals, and the antiviral drug used. In [47], an optimal vaccination strategy includes the effect of migration and impulsive travel for a COVID-19 epidemic model. In [24] and [32], vaccine administration strategies are studied by solving optimal control problems. In [42], optimal controllers are designed considering both vaccination and social distancing. However, traditional optimal control strategies often encounter difficulties when dealing with complex, nonlinear, and uncertain real-world challenges, primarily due to their reliance on analytical calculations for determining optimal solutions. Hence, in recent times, researchers have also begun employing metaheuristic techniques to refine control parameters [6, 29, 41]. Inspired by nature, these metaheuristic techniques offer approximate solutions to complex problems by integrating constructive methods with local and population-based search strategies, along with mechanisms to escape local optima [46]. Accordingly, they have been employed to optimize COVID-19 controllers. For instance, in [1], a genetic algorithm optimizes an Adaptive-Network-based Fuzzy Inference System (ANFIS) to control the number of infected and suspected individuals by isolation and vaccination rates. In our earlier work [38], we also utilized genetic algorithms to optimize the membership functions of a type-2 fuzzy controller designed for controlling the spread of COVID-19.

However, theoretical control strategies that overlook real-world constraints tend to be impractical. Hence, some studies have considered vaccination limitations when designing the control strategy. For example, considering the limited supply of vaccines for influenza diseases in Mexico, the vaccination strategies in [14] are defined using age-targeted allocations. In [4], a simplified Susceptible Infected Recovered Deceased (SIRD) model is used for COVID-19 modeling. The vaccination prioritization for heterogeneous populations is formulated as an optimal control problem and solved by Pontryagin's Maximum Principle. In [24], based on an SIR model, vaccination allocation is formulated as both a single- and multi-objective optimal control problem. The single-objective problem tries to minimize the number of infected individuals, whereas the multi-objective problem minimizes both the infected population and vaccination concentration. In [32], a modified SEIR model is considered for COVID-19 modeling. Four scenarios are considered based on the vaccination limitation for each day and the total simulation duration, and are formulated as the optimal control problem. Finally, in [19], an optimization control problem is designed for vaccination allocation to different age groups.

3 Preliminaries on S^{2}EIAR model

The Stochastic SEIAR (S^{2}EIAR) model in [38] for the COVID-19 spread is presented here. The S^{2}EIAR model includes parameter and variable uncertainties and can better present real-world situations. The overall structure of the S^{2}EIAR model is illustrated in Figure 1, and its dynamics are presented as follows [38]:

$$S[k+1] = \tilde{S}[k] - \tilde{\beta}[k](\tilde{\varepsilon}[k]\tilde{E}[k] + (1-\tilde{q}[k])\tilde{I}[k] + \tilde{\delta}[k]\tilde{A}[k])\tilde{S}[k] - \tilde{S}[k]u_{Va}, \tag{1}$$

$$E[k+1] = \tilde{E}[k] + \tilde{\beta}[k](\tilde{\varepsilon}[k]\tilde{E}[k] + (1-\tilde{q}[k])\tilde{I}[k] + \tilde{\delta}[k]\tilde{A}[k])\tilde{S}[k] - \tilde{\kappa}[k]\tilde{E}[k], \tag{2}$$

$$I[k+1] = \tilde{I}[k] + \tilde{\rho}[k]\tilde{\kappa}[k]\tilde{E}[k] + (1-\tilde{z}[k])\tilde{\eta}[k]\tilde{A}[k] - \tilde{\alpha}[k]\tilde{I}[k] - \tilde{I}[k]u_{Is}, \tag{3}$$

$$A[k+1] = \tilde{A}[k] + (1-\tilde{\rho}[k])\tilde{\kappa}[k]\tilde{E}[k] - \tilde{\eta}[k]\tilde{A}[k], \tag{4}$$

$$R[k+1] = \tilde{R}[k] + \tilde{z}[k]\tilde{\eta}[k]\tilde{A}[k] + \tilde{f}[k]\tilde{\alpha}[k]\tilde{I}[k], \tag{5}$$

$$N[k] = \tilde{S}[k] + \tilde{E}[k] + \tilde{I}[k] + \tilde{A}[k] + \tilde{R}[k], \tag{6}$$

where $S[k]$ is the susceptible (but not yet infected), $E[k]$ indicates the exposed (infected but not yet infectious), $I[k]$ denotes infected (symptomatic), $A[k]$ is asymptomatic (infected without symptoms), and R indicates the recovered population. All variables S, E, I, A, and R are normalized by dividing by the population size N, which confines them to the range of [0,1]. Also, u_{Va} and u_{Is} indicate the vaccination and isolation rates, respectively. Eqs. 3 and 4 indicate that exposed individuals are categorized into two groups based on a rate, $\tilde{\kappa}$: the infected and the asymptomatic. Specifically, a fraction $\tilde{\rho}$ of the exposed individuals transitions to the infected group, while a fraction of $1-\tilde{\rho}$ enters the asymptomatic group. From the asymptomatic group, a portion $\tilde{z}$ eventually recovers at a specified rate $\tilde{\eta}$, as outlined in Eq. 5. Simultaneously, the remaining fraction, $1-\tilde{z}$, reverts to the infected group at the same rate described in Eq. 3. Furthermore, as stated in Eq. 3, infected individuals exit their group at a rate $\tilde{\alpha}$, with a portion of $\tilde{f}$ recovering and the remainder, $1-\tilde{f}$, dying due to the illness. As seen from Eq. 1 and Eq. 3, this model applies the vaccination administrations to the suspected population and isolates the infected population. The $\sim$ on the parameters and variables shows their uncertainty by a small random number around their mean value. In other words, denote $\underline{x}[k] = [S, E, I, A, R]^T$ and $\underline{\Pi} = [\beta, \varepsilon, q, \delta, \rho, \kappa, z, \eta, \alpha, f]^T$ as the vectors of variables and parameters, then their perturbed values are attained as [38]:

$$\tilde{x}[k] = \underline{x}[k] + \mathfrak{N}\underline{n} \times \underline{x}[k],\ \tilde{\Pi}[k] = \underline{\Pi} + \mathfrak{M}\underline{m} \times \underline{\Pi}, \tag{7}$$

where $\underline{n} \in \mathbb{R}^5$ and $\underline{m} \in \mathbb{R}^{10}$ stand for measurement uncertainties in the real world and have elements in $\mathcal{N}(0,1)$, with $\mathcal{N}(0,1)$ as the normal distribution with mean zero and variance 1. The sign $\times$ represents the element-by-element product, and $\mathfrak{N}$ and $\mathfrak{M}$ are additive perturbation constants.

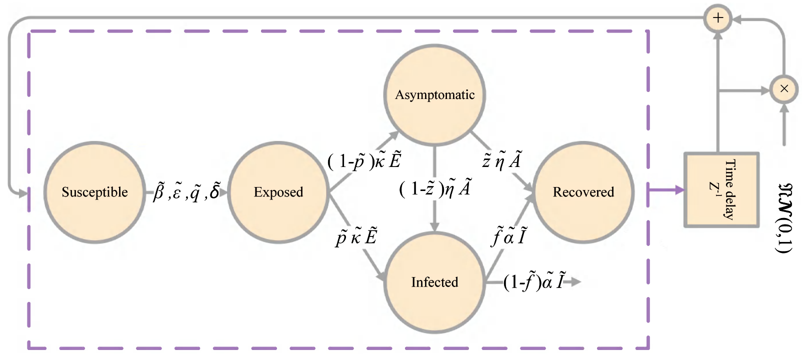

Figure 1: The structure of the Stochastic SEIAR (S^{2}EIAR) model for COVID-19 spread, as proposed in [38]. This model incorporates parameter and variable uncertainties to represent real-world epidemic dynamics better.

Remark 3.1. *The S^2EIAR model, outlined in* [38]*, expands on the foundational equations of the SEIAR model discussed in* [1] *and* [27] *by incorporating uncertainties. A detailed analysis of the SEIAR model is presented in* [27]*, which includes an evaluation of the reproduction number, R_0, and the overall stability of the system's dynamics (refer to Section 2 of* [27]*). By utilizing the Jacobian matrix derived from linearization, it is shown that in the absence of control measures (i.e., when $u_{Va} = u_{Is} = 0$), the equilibrium points are globally asymptotically stable. Moreover, in the presence of control inputs—vaccination (u_{Va}) and isolation signals (u_{Is})—it is mathematically demonstrated in* [1] *that the susceptible population S, along with E, I, and A, converge to zero as $k \to \infty$. This convergence result can be readily inferred from the dynamics outlined in Eqs. (1)-(5), given that all physical signals, including control inputs, are constrained within the range of* $[0, 1]$.

4 The proposed method

This section describes the proposed VIETFC approach and its optimization procedure.

4.1 Control of COVID-19

Here, a type-2 fuzzy controller is designed that determines the vaccination and isolation rates according to their upper limits, $\overline{U}_{Va}$ and $\overline{U}_{Is}$, respectively, and the number of infected individuals, $I[k]$. In other words, u_{Va} and u_{Is} in Eq. 1 and Eq. 3 are denoted by $u_{Va}(I[k], \overline{U}_{Va}, \overline{U}_{Is})$ and $u_{Is}(I[k], \overline{U}_{Va}, \overline{U}_{Is})$.

This differs from the study in [38] where u_{Va} and u_{Is} were functions of $e[k]$ and $\Delta e[k]$ with $e[k] = (I_d[k] - \tilde{I}[k])/N[k]$ and $I_d[k]$ as the desired infected population at time k.

Hence, the following fuzzy rules are defined:

$$\text{If } I[k] \text{ is } \tilde{A}_1^l \text{ and } \overline{U}_{Va}[k] \text{ is } \tilde{A}_2^l \text{ and } \overline{U}_{Is}[k] \text{ is } \tilde{A}_3^l, \text{ then } \upsilon[k] \text{ is } \tilde{B}_1^l \text{ and } \imath[k] \text{ is } \tilde{B}_2^l, \tag{8}$$

where $\tilde{A}_i^l$, $i = 1, 2, 3$ is the i^{th} interval type-2 fuzzy set of the fuzzy rule's antecedent, and $\tilde{B}_1^l$ and $\tilde{B}_2^l$ are the interval type-2 fuzzy sets of the l^{th} fuzzy rule's consequent with $l = 1, \ldots, M$. The fuzzy system's outputs, $\upsilon[k]$ and $\imath[k]$, are the coefficients determining the fraction of vaccination and isolation upper bounds, respectively, to be applied to the model as the control input.

The proposed fuzzy controller uses a singleton fuzzifier, product inference engine, Karnik-Mendel type-reduction, and Centroid defuzzifier. The following equations attain the fuzzy system's output:

$$\begin{aligned}
F_\ell(u|W) &= \frac{\sum_{l=1}^{L} \overline{W}_\ell^l \overline{f}^l + \sum_{l=L+1}^{M} \overline{W}_\ell^l \underline{f}^l}{\sum_{l=1}^{L} \overline{f}^l + \sum_{l=L+1}^{M} \underline{f}^l} = W_\ell^T \phi_\ell, \\
F_\imath(u|W) &= \frac{\sum_{l=1}^{R} \overline{W}_\imath^l \underline{f}^l + \sum_{l=R+1}^{M} \overline{W}_\imath^l \overline{f}^l}{\sum_{l=1}^{R} \underline{f}^l + \sum_{l=R+1}^{M} \overline{f}^l} = W_\imath^T \phi_\imath, \\
[\upsilon[k], \imath[k]]^T &= \frac{F_\ell(u|W) + F_\imath(u|W)}{2} = \frac{1}{2}(W^T \phi),
\end{aligned} \tag{9}$$

Algorithm 1 Optimization procedure of the proposed VIETFC for S^2EIAR model.

Input: Fuzzy system ($\mathscr{F}$), Max generation ($\mathscr{G}$), Population size ($\mathscr{P}$), Mutation rate ($\mathscr{M}$), Crossover rate ($\mathscr{C}$)
Output: Optimized fuzzy system ($\mathscr{F}_o$)
Initialization:
  Set S^2EIAR parameters
  Set S, E, I, A, and R populations
  Generate feasible solutions randomly
repeat
  Cost Evaluation
  Parent selection
  Crossover operation
  Mutation operation
until stop conditions are met

---

where $u = [I[k], \overline{U}_{Va}[k], \overline{U}_{Is}[k]]^T \in \mathbb{R}^3$ is the fuzzy system's input vector, $\underline{f}^l = \prod_{i=1}^{3} \underline{\mu}_{A_i^l}(u(i)), \overline{f}^l = \prod_{i=1}^{3} \overline{\mu}_{A_i^l}(u(i))$, where $\underline{\mu}_{A_i^l}(u(i))$ and $\overline{\mu}_{A_i^l}(u(i))$ indicate, respectively, the lower and upper membership functions of $\mu_{\tilde{A}_i^l}(u(i))$ with $(i = 1, \ldots, 3)$. Also, $W = [W_l^T, W_r^T]^T$, $W_\ell^T = [\overline{W}_\ell^1, \ldots, \overline{W}_\ell^M]$, and $W_r^T = [\overline{W}_r^1, \ldots, \overline{W}_r^M]$ in which $\overline{W}_\ell^l = [\overline{W}_{\ell v}^l, \overline{W}_{\ell i}^l]^T$ and $\overline{W}_r^l = [\overline{W}_{rv}^l, \overline{W}_{ri}^l]^T$ are the center of the interval sets of the l^{th} fuzzy rule's consequent, R, and L are switching points and satisfy $\overline{W}_\ell^L \le F_\ell \le \overline{W}_\ell^{L+1}$ and $\overline{W}_r^R \le F_r \le \overline{W}_r^{R+1}$. The fuzzy basis functions vector is defined by $\phi = [\phi_\ell^T, \phi_r^T]^T$ with $\phi_\ell = [\varphi_l^1, \varphi_l^2, \ldots, \varphi_l^M]^T$, $\phi_r = [\varphi_r^1, \varphi_r^2, \ldots, \varphi_r^M]^T$, $\varphi_\ell^i = [\overline{f}^i/D_\ell, \underline{f}^i/D_\ell]$, $D_\ell = \sum_{i=1}^{L} \overline{f}^i + \sum_{i=L+1}^{M} \underline{f}^i$, $\varphi_r^i = [\underline{f}^i/D_r, \overline{f}^i/D_r]$, $D_r = \sum_{i=1}^{R} \underline{f}^i + \sum_{i=R+1}^{M} \overline{f}^i$.

The vaccination and isolation rates are then computed as:

$$u_{Va}[k] = v[k]\overline{U}_{Va}[k],\ u_{Is}[k] = i[k]\overline{U}_{Is}[k]. \tag{10}$$

The structure of the proposed VIETFC is illustrated in Figure 2. As can be seen, the upper bound calculator block receives the daily upper bounds on isolation and vaccination determined by the authorities/policymakers. The fuzzy system's outputs determine the fraction of these upper bounds to be applied as the daily vaccination administration of the suspected population or the isolation rate of the infected population. Similar to [38], here the number of infected individuals is normalized by dividing by the population size. The dashed lines depict the optimization of the proposed controller by the genetic algorithm.

4.2 Optimization of the proposed VIETFC

The fuzzy controller's parameters are optimized using a genetic algorithm to minimize the total number of infected individuals over a T-day simulation period. The optimization problem is formulated as:

$$\min_{\boldsymbol{\theta}} \ J(\boldsymbol{\theta}) = \sum_{k=1}^{T} I[k; \boldsymbol{\theta}], \tag{11}$$

where:

- $\boldsymbol{\theta}$ denotes the vector of tunable controller parameters (including input/output membership functions and rule weights),
- $I[k; \boldsymbol{\theta}]$ represents the number of infected individuals at time step k, attained from Eq. (3), under the control policy defined by $\boldsymbol{\theta}$,
- $J(\boldsymbol{\theta})$ is the cumulative infection cost over the simulation horizon.

The genetic algorithm iteratively updates the controller parameters by evaluating the cost function over successive generations. A population-based search strategy is used, where candidate solutions are selected, recombined, and mutated to efficiently explore the parameter space. Parallel execution and cost monitoring mechanisms are employed to accelerate convergence and guide the search toward an optimal control policy.

Algorithm 2 Cost function.

Input: Candidate fuzzy system ($\mathscr{F}_c$), S^{2}EIAR Model, Scenario, Number of simulation days ($\mathscr{D}$)
Output: Cost
for k in $\mathscr{D}$ **do**
    Simulation based on yesterday's variables
    $I[k]$ calculation
    Control signal generation:
        $u_{Va}, u_{Is} = \mathscr{F}_c(I[k], \overline{U}_{Va}, \overline{U}_{Is}) \times [\overline{U}_{Va}, \overline{U}_{Is}]$
end for
Return Sum(I)

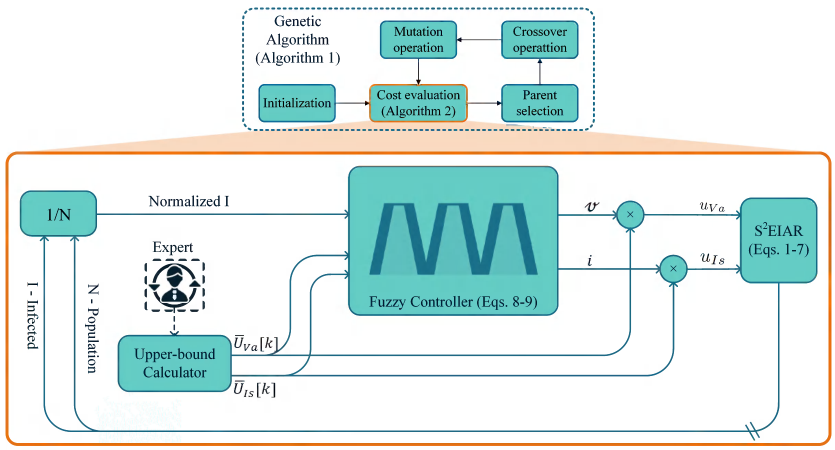

Figure 2: Structure of the proposed VIETFC. The dotted line represents the optimization of the fuzzy system using a genetic algorithm, while the dashed line indicates the upper bound on isolation and vaccination rates as specified by the expert authorities. Candidate solutions are evaluated each generation through population valuation and cost analysis, with performance measured by infection control effectiveness over 60 days.

The complexity is dominated by the genetic algorithm tuning and epidemic model simulation. With population size P, generations G, and simulation length T, each tuning requires $O(P \times G \times T)$ operations. Parallelization reduces runtime without affecting complexity.

5 Results

Here, the proposed VIETFC is examined under four scenarios where the vaccination rate of suspected and isolation rate of infected population are limited by 1) a fixed upper bound during the time interval, 2) a time-varying upper bound during the time interval, 3) a total limited vaccination and isolation rates during the time interval, and 4) a time-varying upper bound during the time interval with a total limited isolation and isolation rates (considering both case 2 and 3).

The proposed VIETFC is implemented in MATLAB (2023a) on a system with a Core i7 CPU and 16 GB RAM, and the source code is released on GitHub[1]. The model parameters are derived from [1, 27], as illustrated in Table 1. The total simulation period is $T = 60$ days. The variables of Eqs. (1)-(6) are initialized to $S[0] = 0.9$, $I[0] = 0.1$, $N[0] = 1$, and $E[0] = A[0] = R[0] = 0$, as referenced in [1]. All variables are constrained to the range of [0, 1]. The additive perturbation constants $\mathfrak{N}$ and $\mathfrak{M}$ are 0.01. Each input and output variable utilizes two Gaussian membership functions, initialized with centers at 0 and 1 with supports extending up to 1.2.

To design a fuzzy logic controller for a critical application like COVID-19 control, it is essential to maintain simplicity, interpretability, and computational efficiency while ensuring the system remains effective. In this design, each input dimension is represented by three Gaussian fuzzy sets: "Low", "Medium", and "High." Gaussian membership functions are chosen for their smooth and differentiable properties. Specific fuzzy operators are selected to ensure smooth and efficient processing. Aggregation, which combines the outputs of individual rules, uses summation, allowing for a more

[1] https://github.com/salehiali1374/VIETFC

Table 1: Standard model parameter settings.

Parameter	Value	Parameter	Value	Parameter	Value	Parameter	Value
κ	0.54	f	0.965	β	1	q	0.5
ρ	0.1	ε	0	α	0.3	δ	1
η	0.3	z	0.02				

expressive output. Implication, which determines how the antecedent of a rule affects the consequent, employs the production (multiplication) method, scaling the consequent fuzzy set by the degree of fulfillment of the antecedent. Similarly, the AND method combines multiple conditions in the antecedent and uses production, ensuring strict and smooth transitions between rules. The parameters for both input and output fuzzy sets are initialized in $[0, 1]$.

For each scenario, the simulations are performed for sixty days. The total number of fuzzy rules is also attained via optimization. The genetic algorithm's population size, generation, elitism population, mutation rate, and crossover rate are set to 100, 50, 5, 0.1, and 0.8, respectively, by trial and error. The optimization process is repeated 10 times, and the best results are derived. The robustness of the fuzzy system in the presence of uncertainties, such as different parameters of the model due to different COVID-19 variants, is also studied for $\kappa = 0.25, 0.75$, and $q = 0.25, 0.75$ without reoptimizing the proposed controller.

Three metrics are defined to evaluate how the proposed method performs in infected population reduction, vaccination administration amount, and isolation cases. Tables 2-5 depicts the metrics for all four scenarios with different q and κ.

$$M_1 = \sum_{k=1}^{60} I[k],\ M_2 = \sum_{k=1}^{60} u_{Va}[k],\ M_3 = \sum_{k=1}^{60} u_{Is}[k]. \tag{12}$$

For comparison purposes, a PID controller (Appendix I) and a type-1 fuzzy system (Appendix II) are designed similarly. The three metrics are calculated for them. Comparing M_1-M_3 in Tables 2-5, the PID controller achieves a lower M_1 than VIETFC by increasing vaccinations (resulting in a higher M_2). For instance, as Figure A.3 depicts, the PID controller consumes all the vaccination capacity on the first day of the pandemic to reduce the infected population.

5.1 Scenario 1 – with constant instant isolation and vaccination rate constraint

The administration of vaccinations is notably influenced by various constraints within the healthcare system, including the capacity of healthcare facilities, the availability of medical personnel, and the adequacy of vaccine storage facilities. As a result, the daily number of administered vaccines is limited. To deal with such a limitation, in scenario 1, both the isolation rates of the infected population and the vaccination rates for the suspected population are assumed to be restricted by fixed upper bounds. The following constraints are considered for them:

$$u_{Va}[k] < \overline{U}_{Va} = cte,\ u_{Is}[k] < \overline{U}_{Is} = cte, \tag{13}$$

where $\overline{U}_{Va}$ and $\overline{U}_{Is}$ are considered fixed, indicating a constant limitation of isolation and vaccination administration for infected and suspected populations during the time interval.

Figure 3 illustrates the type-2 fuzzy controller surfaces for vaccination fraction (υ) concerning infection (I) and vaccination upper bound ($\overline{U}_{Va}$) (left) and the fuzzy surface for isolation fraction (i) concerning I and $\overline{U}_{Is}$ (right). As illustrated in Figure 3, the higher υ and i are suggested when the infected population rises. Also, i is directly related to the upper bound of isolation. However, increasing the upper bound of vaccination does not affect υ. In contrast, the type-1 fuzzy controller produces almost a constant output despite input variations (Figure A.5 in Appendix II).

Figure 4 shows the controlled, uncontrolled infected population (mean value and their shaded standard deviation around the mean), the daily cases of vaccination ($\tilde{S}[k]u_{Va}$) and isolation ($\tilde{I}[k]u_{Is}$) and the upper limits of vaccination and isolation rates ($\overline{U}_{Va}$ and $\overline{U}_{Is}$, respectively) for different κ and q. The blue and red shadow curves show the standard deviation from the mean values of the uncontrolled and controlled infected populations, respectively. As can be seen, vaccination and isolation cases peak in the first days of COVID-19 emergence, which is consistent with real-world decisions regarding the emergence of a new disease. As the upper limit is not tightly restricted, the higher amount of vaccination and isolation causes the peak of the infected population to decrease drastically to zero on the 20th day.

Table 2 shows the three metrices,M_1-M_3, of all three controller for the first scenario. As the table shows, the number of infected individuals (M_1) for the proposed method is 0.54, showing that only 54% of the people were infected during the whole period. This result is expected since, in the first scenario, the upper bounds are not too tight, which is

Table 2: Metrics comparison for 1^{st} Scenario

		PID			Type-1 Fuzzy			Type-2 Fuzzy		
κ	q	M_1	M_2	M_3	M_1	M_2	M_3	M_1	M_2	M_3
0.25	0.25	0.4245	0.7628	0.0983	0.5420	0.7163	0.1143	0.5422	0.7271	0.1034
	0.5	0.4261	0.7631	0.0982	0.5412	0.7166	0.1141	0.5418	0.7274	0.1033
	0.75	0.4241	0.7618	0.0983	0.5401	0.7161	0.1138	0.5422	0.7263	0.1034
0.5	0.25	0.4224	0.7622	0.0982	0.5407	0.7164	0.1140	0.5417	0.7267	0.1032
	0.5	0.4289	0.7623	0.0987	0.5420	0.7160	0.1143	0.5438	0.7266	0.1038
	0.75	0.4246	0.7628	0.0982	0.5398	0.7160	0.1138	0.5417	0.7271	0.1033
0.75	0.25	0.4290	0.7612	0.0984	0.5421	0.7156	0.1144	0.5427	0.7256	0.1035
	0.5	0.4254	0.7608	0.0983	0.5398	0.7167	0.1137	0.5421	0.7254	0.1034
	0.75	0.4279	0.7622	0.0984	0.5386	0.7168	0.1135	0.5425	0.7265	0.1034
Change from baseline		0.43±0.00	0.76±0.00	0.10±0.00	-0.26±0.22	0.04±0.05	-0.30±0.26	-0.31±0.06	-0.01±0.09	-0.42±0.08

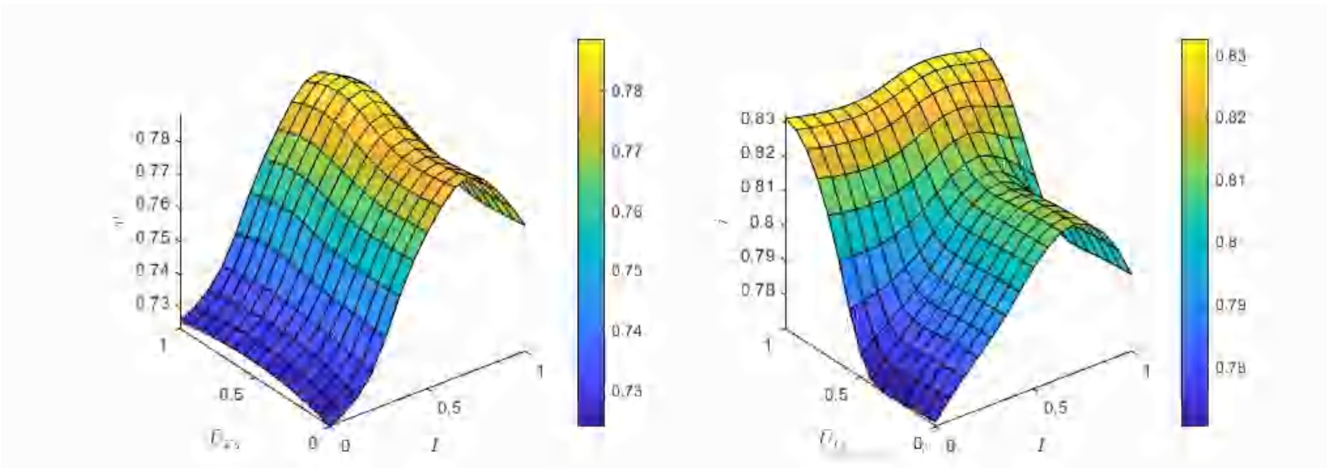

Figure 3: Fuzzy surfaces of the proposed VIETFC for Scenario 1: (left) vaccination fraction (υ) concerning infected population (I) and vaccination upper bound ($\overline{U}_{Va}$); (right) isolation fraction (i) concerning infected population (I) and isolation upper bound ($\overline{U}_{Is}$). This scenario aims to reduce the number of infected individuals while maintaining fixed daily upper bounds for vaccination and isolation.

demonstrated by higher vaccination administration (M_2) for the first scenario compared to the remaining scenarios. In other words, in the first scenario, by vaccinating 72% of the suspected population and isolating 10% of the infected population, only 54% are infected with COVID-19.

The results for different q and κ are almost the same as $q = 0.5$ and $\kappa = 0.5$, which confirms the robustness of the proposed controller in the presence of uncertainties. Also, the table shows that with a 50% change in q and κ, we have, on average, up to 9% standard deviation (STD) compared with the nominal $q = 0.5$ and $\kappa = 0.5$. This result contrasts with the previous work in [38] where uncertainties in q and κ resulted in higher deviation in controller performance.

Comparing the results type-1 and type-2 fuzzy controllers in Table 2, the performance of the type-1 and type-2 fuzzy systems are comparable. This result may be because only one of the fuzzy system inputs is uncertain, and type-1 fuzzy systems can also handle it. The type-2 fuzzy controller has a lower overall variance in M_1 and M_3, which confirms its higher robustness than the type-1 fuzzy controller. The PID controller achieves the lowest M_1 than VIETFC by increasing vaccinations (resulting in a higher M_2). The PID controller tends to focus exclusively on reducing the spread of the disease by concentrating solely on error minimization. In contrast, VIETFC considers the constraints as its input, offering a more comprehensive and flexible solution and a better understanding of the problem.

5.2 Scenario 2 - with time-varying instant isolation and vaccination rate constraint

In a realistic scenario, the rules for vaccination administration and isolation can vary depending on the day of the week. Therefore, in this case, the fixed upper limits for vaccination and isolation in Scenario 1 have been updated to be time-varying, making them more aligned with real-life situations. The constraints can be indicated as follows:

$$u_{Va}[k] < \overline{U}_{Va}[k],\ u_{Is}[k] < \overline{U}_{Is}[k]. \tag{14}$$

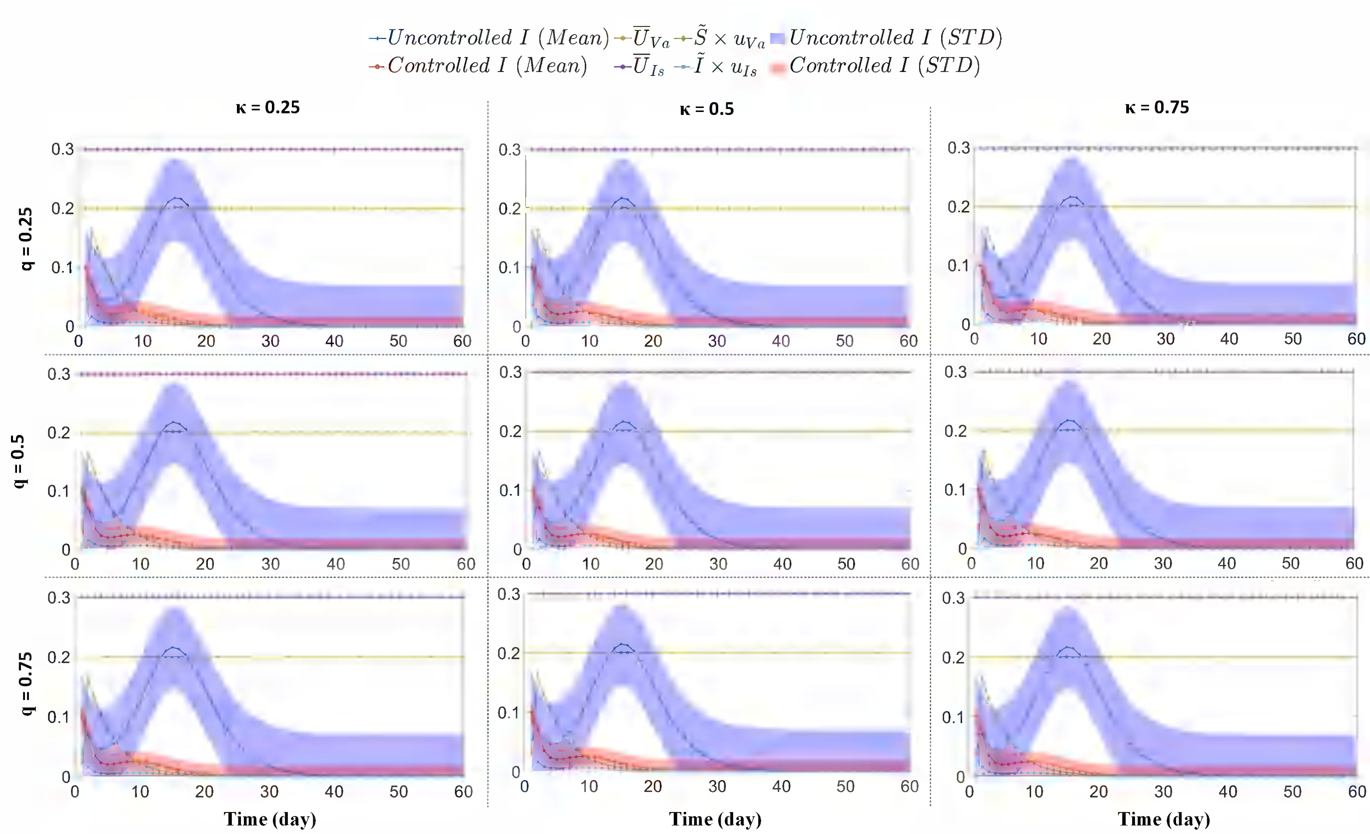

Figure 4: Comparison of the infected population size (controlled, desired, and uncontrolled), vaccination rate, and isolation rate over sixty days with varying values of q and κ in Scenario 1 for the proposed VIETFC. The shaded areas represent the standard deviation around the mean values of the controlled and uncontrolled infected populations.

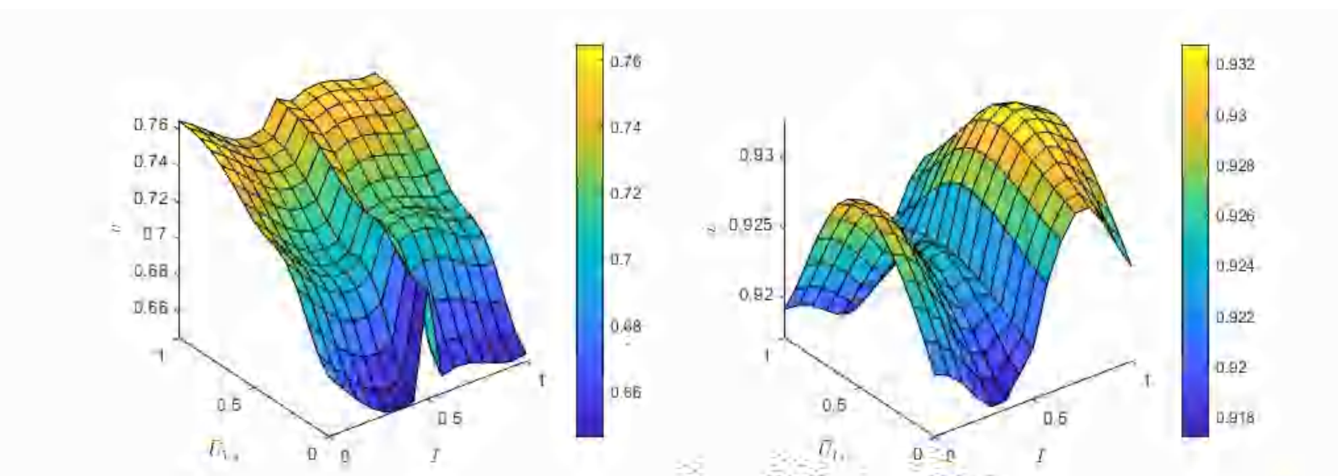

Figure 5: Fuzzy surfaces of the proposed VIETFC for Scenario 2: (left) vaccination fraction (υ) for infected population (I) and vaccination upper bound ($\overline{U}_{Va}$); (right) isolation fraction (ι) for infected population (I) and isolation upper bound ($\overline{U}_{Is}$). This scenario aims to reduce the number of infected individuals while accounting for time-varying daily upper bounds for vaccination and isolation.

Eq. 14 shows that the upper bounds are a function of k. The fuzzy surfaces for vaccination fraction (υ) and isolation fraction (ι) are illustrated in Figure 5 (similar to Figure 3 for Scenario 1). As can be seen, when $\overline{U}_{Va}$ increases, higher υ are suggested. However, υ is not much related to the number of infected individuals (I). This result may be because the vaccination rate u_{Va} is not directly related to I according to Eq. 1, and as the upper bounds are more restricted, the direct effect of $\overline{U}_{Va}$ is much more effective than the indirect effect of I. As the fuzzy surface of the isolation depicts, the

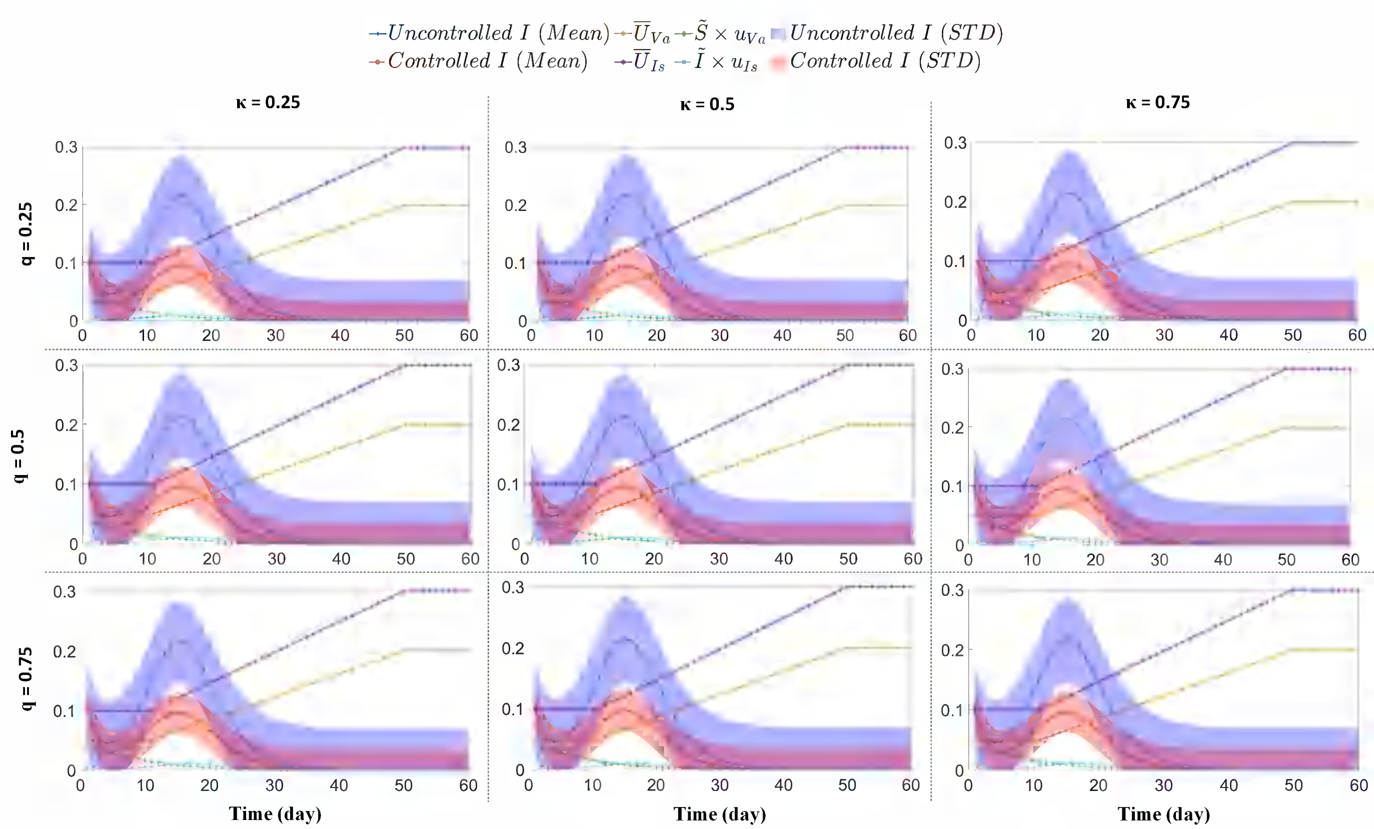

Figure 6: Simulation results for Scenario 2 with varying q and κ over sixty days, showing the daily vaccination ($\tilde{S}[k]u_{Va}$) and isolation ($\tilde{I}[k]u_{Is}$) cases, upper bounds for vaccination ($\overline{U}_{Va}$) and isolation ($\overline{U}_{Is}$) rates, as well as the mean and standard deviation of controlled and uncontrolled infected population. The time-varying upper bounds reflect real-world constraints, with tighter vaccination limits in the early days of the pandemic, followed by gradual increases.

isolation fraction (i) is almost at the highest possible values (0.92-0.93). The fuzzy surface also shows the direct effect of the growth of I on the i. Notably, because of the limited vaccination and isolation, all the capacities for vaccination administration or isolation cases are employed in the first days. Hence, the controller is not optimized for peak values of the infected population (I), occurring in the latter days.

Figure 6 depicts the daily cases of vaccination ($\tilde{S}[k]u_{Va}$) and isolation ($\tilde{I}[k]u_{Is}$) and the upper limits of vaccination ($\overline{U}_{Va}$) and isolation ($\overline{U}_{Is}$) rates as well as the controlled and uncontrolled infected population (mean value and their shaded standard deviation around the mean). As can be seen, $\overline{U}_{Va}$ and $\overline{U}_{Is}$ are time-varying. They are chosen to be small until the 10^{th} day and then increase constantly to reach their maximum bound on the 15th day. These upper bounds match the real-world situations when there are insufficient supplies or inadequate infrastructure in the early stages of the disease. Specifically, vaccination cannot be supplied or produced in the first days of the pandemic, while isolation strategies can be implemented more rapidly. Hence, the upper bound of vaccination is set to be tighter than that of isolation.

Compared to Scenario 1, as the upper bound is more restricted, a smaller vaccination and isolation rate is applied, and the total number of infected individuals (I) is higher than the first scenario, but acceptably lower than the infected cases when no control is applied. The controller employs more vaccinations (on the first days) to reduce the number of infected individuals. According to $M_1 - M_3$ in Table 3, M_1 increases compared to Scenario 1 because of less vaccination administration (M_2) in Scenario 2 due to tighter limitations. M_3 is higher than Scenario 1, which can be because of applying more isolations due to a lower vaccination capacity.

According to Table 3, the PID controller reaches the lowest M_1 among the three controllers by consuming the maximum possible vaccinations (Figure A.2 in Appendix I). In contrast, VIETFC focuses on reducing the vaccination administrations (M_2). The type-1 and proposed type-2 fuzzy controllers have comparable results overall, with a lower variance of the proposed method. All three controllers reduce the number of infected individuals to zero in almost 30 days.

Table 3: Metrics comparison for 2^{nd} Scenario

		PID			Type-1 Fuzzy			Type-2 Fuzzy		
κ	q	M_1	M_2	M_3	M_1	M_2	M_3	M_1	M_2	M_3
	0.25	1.3717	0.4098	0.1565	1.5966	0.3455	0.1620	1.6920	0.3174	0.1611
0.25	0.5	1.3691	0.4090	0.1563	1.5952	0.3456	0.1618	1.6899	0.3168	0.1609
	0.75	1.3804	0.4084	0.1569	1.5955	0.3445	0.1618	1.6955	0.3161	0.1613
	0.25	1.3735	0.4082	0.1569	1.5964	0.3447	0.1619	1.6955	0.3161	0.1613
0.5	0.5	1.3718	0.4086	0.1565	1.6927	0.3470	0.1617	1.6923	0.3165	0.1611
	0.75	1.3723	0.4094	0.1565	1.5957	0.3450	0.1619	1.6909	0.3170	0.1611
	0.25	1.3772	0.4082	0.1566	1.5939	0.3462	0.1618	1.6933	0.3161	0.1611
0.75	0.5	1.3581	0.4089	0.1566	1.5980	0.3454	0.1621	1.6932	0.3165	0.1612
	0.75	1.3764	0.4086	0.1567	1.5921	0.3460	0.1616	1.6940	0.3164	0.1612
Change from baseline		1.37±0.01	0.41±0.00	0.16±0.00	0.17±0.11	-0.47±0.17	0.10±0.09	0.04±0.11	0.01±0.15	0.03±0.08

5.3 Scenario 3 - with constrained total vaccination and isolation rates

In a real-world scenario, the total number of available vaccination resources and isolation cases can be limited. Therefore, this situation assumes that the total vaccination and isolation rates are restricted by fixed upper limits, as shown by Eq. 15. However, there is no daily upper limit imposed on these rates.

$$\sum_{t_1}^{t_F} u_{Va}[k] = cte, \sum_{t_1}^{t_F}[k] = cte. \tag{15}$$

Figure 7 shows the surface of the proposed fuzzy controller for the vaccination (υ) and isolation fraction (ι). As can be seen, υ is not affected by the infected population I, while the rise of $\overline{U}_{Va}$ results in a higher υ. The maximum vaccination occurs when $\overline{U}_{Va}$ is 0.5. Also, the rise of I directly affects the rise of ι.

Figure 8 shows the controlled and uncontrolled infected population, the daily remaining vaccination and isolation supplies ($\overline{U}_{Va}$ and $\overline{U}_{Is}$, respectively), and the daily cases of vaccination ($\tilde{S}[k]u_{Va}$) and isolation ($\tilde{I}[k]u_{Is}$). As illustrated, $\overline{U}_{Va}$ and $\overline{U}_{Is}$ increase initially due to reduced infected (I) and suspected (S) populations in the first days of disease spread, allocating the total vaccination/isolation capacity to fewer people. There is no daily upper bound here, but the total number of vaccinations and isolation rates is limited. Hence, the controller suggests a high value of immunization in the first days of disease emergence, which reduces significantly for the remaining days.

In this case, M_1 in Table 4 is higher for all three controllers compared with the previous two scenarios because of a limited total supply lower than the upper limits of Scenarios 1 and 2. Hence, M_2 and M_3 are much lower than those in previous scenarios. In comparing the controllers, as seen in the previous two cases, both the type-1 and the proposed type-2 controllers demonstrate comparable performance, with VIETFC exhibiting lower variance. The PID controller achieves the lowest M_1 value by exhausting all available vaccination and isolation capacity within the first day of the pandemic (Figure A.3), which is impractical. In contrast, the type-1 fuzzy controller and the proposed VIETFC utilize the resources in less than 5 days (Figure A.10 in Appendix II) and 8 days (Figure 8), respectively. Thus, the proposed VIETFC demonstrates a more realistic source consumption among all three controllers.

5.4 Scenario 4 - with time-varying instant/cumulative isolation and vaccination constraint

This scenario integrates the limitations presented in Scenarios 2 and 3, setting more realistic constraints where total and daily resources are restricted. Hence, alongside the time-varying upper bound specified in Eq. 14, there are also upper bounds on the total number of vaccines and isolation cases, as indicated by Eq. 15.

Figure 9 illustrates the fuzzy surface of the proposed controller for the vaccination (υ) and isolation (ι) fractions. As can be seen, with the growth of $\overline{U}_{Va}$ and $\overline{U}_{Is}$, higher υ and ι are suggested. However, a rise in the infected population (I) does not affect υ and ι. This result is reasonable because, due to both limited daily upper bounds and limited total supply, all possible vaccination/isolation are employed on the first days, and the controller is not optimized for higher values of the infected population occurring in the following days.

Figure 10 explains daily vaccination ($\tilde{S}[k]u_{Va}$) and isolation ($\tilde{I}[k]u_{Is}$) cases, the upper bounds of the vaccination and isolation rates ($\overline{U}_{Va}$ and $\overline{U}_{Is}$, respectively), and the number of controlled and uncontrolled infected individuals. As can be seen, the infected population curve (I) is similar to Scenario 3, but with a higher peak and an earlier time

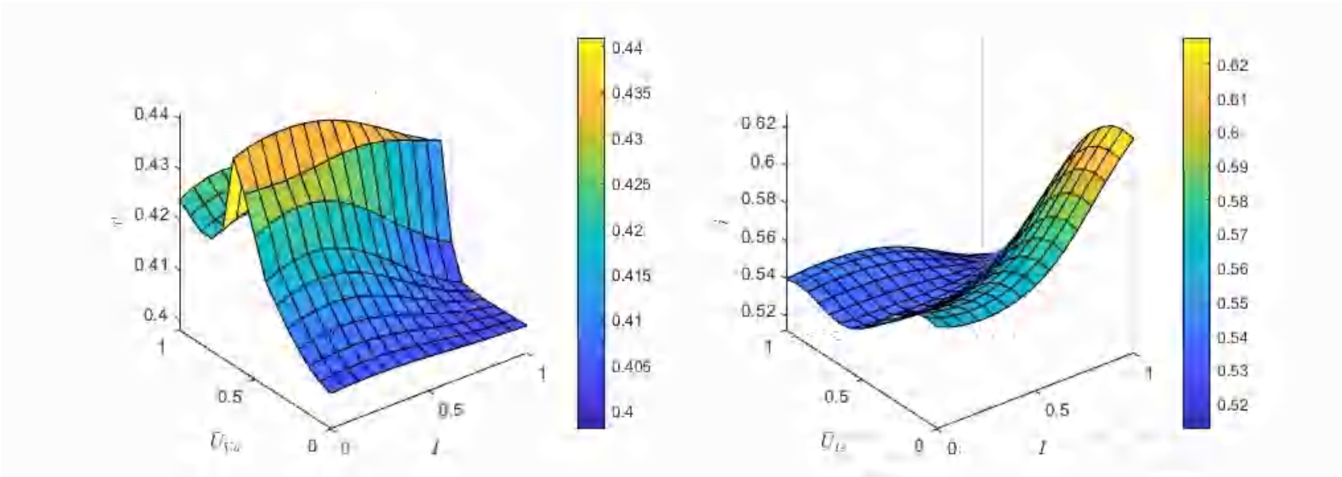

Figure 7: The fuzzy surface of the proposed VIETFC for Scenario 3: (left) The fuzzy surface of the vaccination fraction (v) for I and $\overline{U}_{Va}$, (right) The fuzzy surface of the isolation fraction (i) for I and $\overline{U}_{Is}$. In this scenario, the goal is to minimize the number of infected individuals with limited vaccination and isolation supplies. The vaccination fraction (v) is unaffected by the number of infected individuals (I), while the isolation fraction (i) increases as I rises.

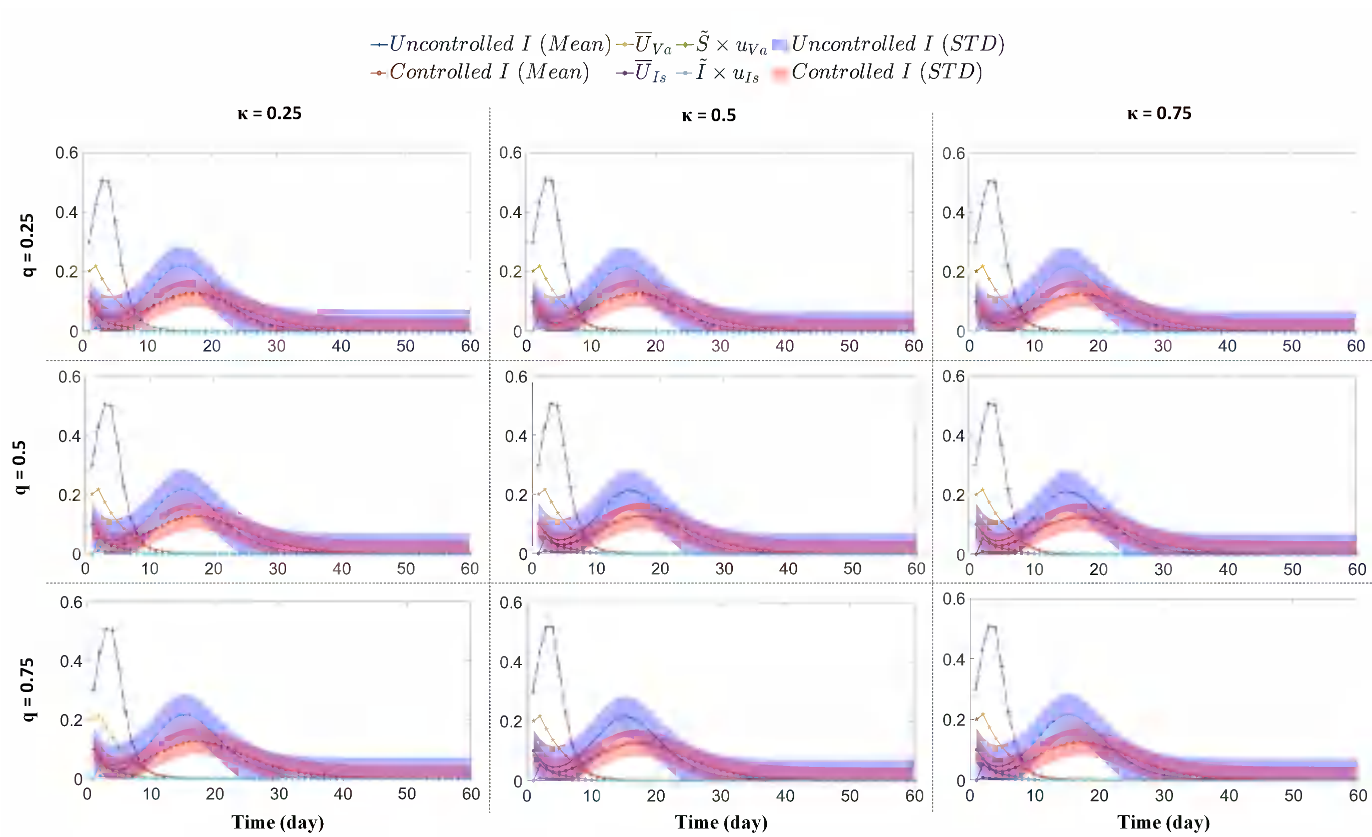

Figure 8: Simulation results of Scenario 3 for various q and κ settings over sixty days for the proposed VIETFC. In the initial days of disease spread, $\overline{U}_{Va}$ and $\overline{U}_{Is}$ increase as the infected (I) and suspected (S) population decrease, allowing for higher vaccination and isolation rates. However, as the supply is limited, the controller suggests high vaccination in the early stages, which significantly reduces in later days.

to reach $I = 0$. This result can be reasonable because the initial lower limits of Scenario 2 on vaccination prevent early vaccination, leading to a higher peak than Scenario 3.

According to the data presented in Table 5, the total values of $M_1 - M_3$ for Scenarios 3 and 4 are comparable due to similar constraints on vaccination and isolation. The primary distinction between the controllers lies in their resource

Table 4: Metrics comparison for 3^{rd} Scenario

		PID			Type-1 Fuzzy			Type-2 Fuzzy		
κ	q	M_1	M_2	M_3	M_1	M_2	M_3	M_1	M_2	M_3
0.25	0.25	2.4990	0.18	0.03	2.5507	0.18	0.03	2.5443	0.18	0.03
	0.5	2.5042	0.18	0.03	2.5475	0.18	0.03	2.5513	0.18	0.03
	0.75	2.5041	0.18	0.03	2.5497	0.18	0.03	2.5462	0.18	0.03
0.5	0.25	2.5003	0.18	0.03	2.5535	0.18	0.03	2.5523	0.18	0.03
	0.5	2.5063	0.18	0.03	2.5500	0.18	0.03	2.5509	0.18	0.03
	0.75	2.5073	0.18	0.03	2.5512	0.18	0.03	2.5504	0.18	0.03
0.75	0.25	2.5027	0.18	0.03	2.5516	0.18	0.03	2.54661	0.18	0.03
	0.5	2.4911	0.18	0.03	2.5468	0.18	0.03	2.54631	0.18	0.03
	0.75	2.4925	0.18	0.03	2.5475	0.18	0.03	2.54959	0.18	0.03
Change from baseline		2.50±0.01	0.18±0.00	0.03±0.00	0.00±0.09	0	0	-0.09±0.11	0	0

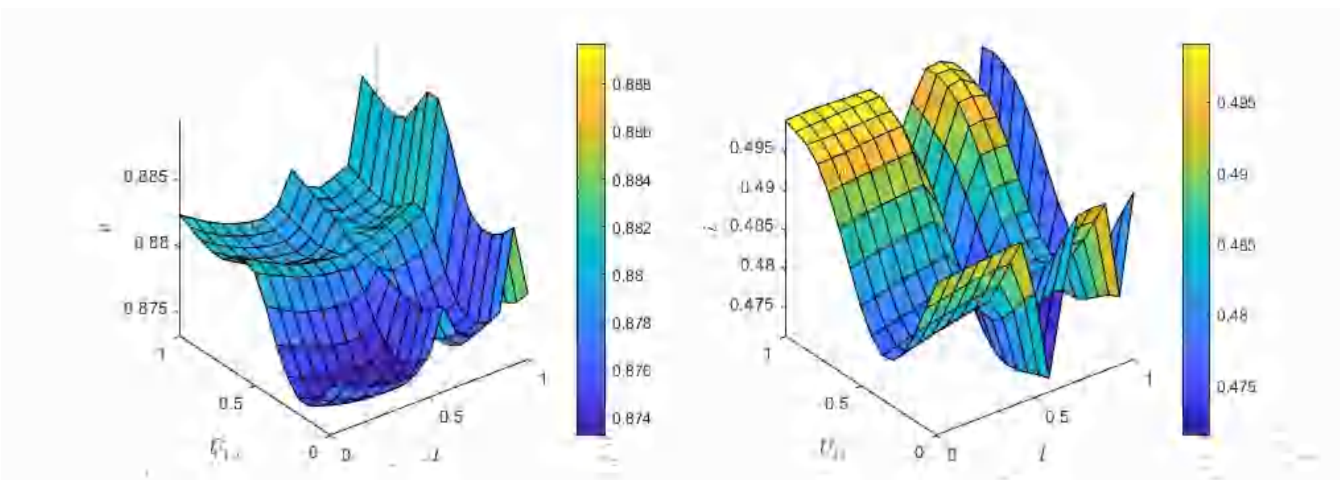

Figure 9: The fuzzy surface of the proposed VIETFC for Scenario 4: (left) the fuzzy surface of the vaccination fraction (υ) concerning I and $\overline{U}_{Va}$; (right) the fuzzy surface of the isolation fraction (i) for I and $\overline{U}_{Is}$. The goal in the fourth scenario is to reduce the number of infected individuals in the presence of both limited supplies and time-varying daily upper bounds for vaccination and isolation rates.

allocation: the PID controller depletes all resources within the first week of the pandemic (as illustrated in Figure A.4), while the type-1 fuzzy controller utilizes its resources over the first 10 days (as shown in Figure A.12). In contrast, the proposed VIETFC controller distributes its resource consumption over the first two weeks (depicted in Figure 10). These results indicate that the proposed method offers a more realistic and practical source allocation while addressing real-world limitations.

6 Discussion

A fuzzy-based control system has been established to address pandemic diseases. Unlike traditional methods, these intelligent and interpretable controllers adeptly manage data and uncertainties, making them well-suited for policy-making in disease control. Compared with the previous work in [38], we address this research's input limits, isolation capacity, and vaccination administration and incorporate them directly into the fuzzy system design. The limitations are studied under four scenarios: fixed daily upper bounds, time-varying upper bounds with a tighter limit in the early days, total isolation capacity/ vaccination administration limit, and finally, both daily upper bounds and total capacity/administration restrictions.

In Scenarios 1 and 2, the lack of total resource limitations enables a greater number of vaccinations and isolation measures, significantly reducing infections during the initial days. However, the stricter restrictions in Scenario 2 lead

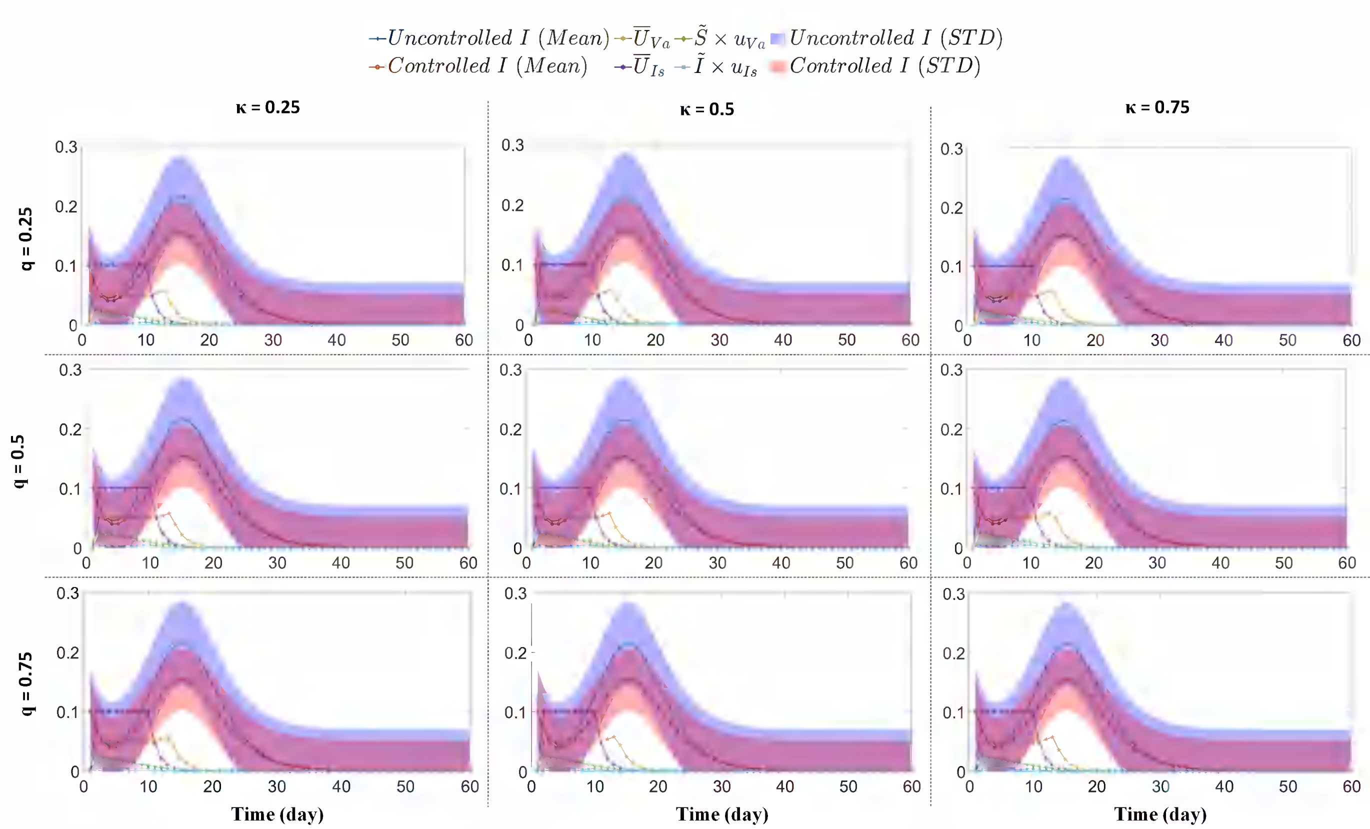

Figure 10: Simulation results of Scenario 4 for various q and κ settings over sixty days for the proposed VIETFC. The infected population curve (I) shows a higher peak and an earlier time to reach $I = 0$ compared to Scenario 3. This result is due to the lower initial limits on vaccination in Scenario 2, which delays vaccination administration and results in a higher peak.

Table 5: Metrics comparison for 4^{th} Scenario

		PID			Type-1 Fuzzy			Type-2 Fuzzy		
κ	q	M_1	M_2	M_3	M_1	M_2	M_3	M_1	M_2	M_3
0.25	0.25	2.5151	0.18	0.03	2.5274	0.18	0.03	2.5423	0.1794	0.03
	0.5	2.5039	0.18	0.03	2.5275	0.18	0.03	2.5376	0.1793	0.03
	0.75	2.5135	0.18	0.03	2.5223	0.18	0.03	2.5351	0.1794	0.03
0.5	0.25	2.54975	0.18	0.03	2.5236	0.18	0.03	2.5380	0.1793	0.03
	0.5	2.5097	0.18	0.03	2.5199	0.18	0.03	2.5354	0.1794	0.03
	0.75	2.5078	0.18	0.03	2.5240	0.18	0.03	2.5407	0.1794	0.03
0.75	0.25	2.5101	0.18	0.03	2.5228	0.18	0.03	2.5372	0.1793	0.03
	0.5	2.4998	0.18	0.03	2.5275	0.18	0.03	2.5368	0.1794	0.03
	0.75	2.5091	0.18	0.03	2.5237	0.18	0.03	2.5403	0.1793	0.03
Change from baseline		2.51±0.01	0.18±0.00	0.03±0.00	0.19±0.08	0	0	0.12±0.09	-0.02±0.02	0

to a slower decline, with zero infections achieved by day 30, compared to just 20 days in Scenario 1 (Figure 4 and Figure 6). In Scenario 3, resource constraints result in a higher peak of the infected population. Yet, the absence of a daily upper limit allows for maximum implementation of measures in the early days (Figure 8). Scenario 4 represents more realistic conditions by incorporating both daily and total resource constraints. Although the early limited resources in this scenario resulted in the highest number of infected individuals, it remains possible to reduce the count to zero after 40 days (Figure 10), much like the outcome seen in Scenario 3.

We further study the performance of the proposed VIETFC in the presence of a known specific noise level in the S^2EIAR model. Therefore, an investigation should clarify the effect of noise in variables such as S and I on the advised control policy and vaccination and isolation output decisions. Also, fuzzy systems can interpret the uncertainties within data [36, 37, 40]. This interpretation enables further analysis and fine-tuning of the controllers' design.

As most pandemics share similar restrictions, the proposed control strategy can be extended to similar pandemic diseases. Another aspect of this research could include multi-agent modeling and control to include variations in infection rates in different parts of a country, affecting total infection relatively [21]. For example, dense populations in some cities increase the number of infected individuals in the country. Hence, the overall policy may not be optimal for other cities. Multi-agent systems can model and control the progress of the disease in different regions with unique agents that communicate with each other to achieve optimal performance and resource utilization.

7 Conclusions

This paper studies the type-2 fuzzy control of the spread of pandemics, COVID-19, as a recent case study, addressing limited vaccination and isolation resources. The S^2EIAR model in [38] is considered for the COVID-19 model. It includes both parameter and variable uncertainties. The number of infected individuals and limitations on vaccination and isolation are fed to a fuzzy system. The fuzzy system then determines the appropriate fraction of vaccination and isolation. The fuzzy system parameters and rules are optimized using a genetic algorithm. The proposed VIETFC is evaluated under four scenarios. The first scenario considers fixed daily upper bounds for the isolation and vaccination rates. The second scenario evaluates tighter daily limits on the first days and gradually reduces the daily limits until the last days. The third scenario considers a total limited resource with no daily limitations, while the fourth scenario combines the variable daily limit in Scenario 2 with the total constrained resource of Scenario 3.

The simulation results show that the proposed VIETFC reaches the lowest infected population in Scenario 1 by applying higher vaccination administration because of fewer resource limitations. Specifically, only 54% of people are infected during the pandemic period by vaccinating 72% of the suspected population. The restrictions are tighter from Scenario 2 to Scenario 4, resulting in a higher infected population due to lower vaccination and isolation. Compared with a PID controller, VIETFC provides a more intuitive and flexible approach that considers the constraints of real-world situations. Conversely, the PID controller primarily aims to minimize the infected population, with impractical source utilization. VIETFC also yields a lower standard deviation and offers more interpretable outputs than a type-1 fuzzy controller. Our approach proves to be a valuable resource for policymakers, enabling them to explore unprecedented scenarios and better prepare for potential future pandemics, ultimately facilitating the development of innovative solutions for effective management.

7.1 Limitations

Although the proposed method demonstrates promising results, particularly in handling the uncertainties associated with pandemics, the optimization process—particularly genetic algorithms—may be prone to overfitting the specific simulation data. This overfitting could impede the model's adaptation to diverse or evolving pandemic conditions. Furthermore, the controller has only been tested within the S^2EIAR model under the assumption of zero population growth, which may not realistically reflect real-world scenarios and could consequently limit its effectiveness in practical applications.

7.2 Suggested future works

In the future, we hope to address longer-term policy making by including population growth models. We also hope to study the data overfitting phenomenon that often occurs with optimization processes, hence reaching more robust policies. Furthermore, viruses also mutate rapidly and hence change behaviors during any given pandemic. Hence, adaptive strategies of uncertain models could be a viable next research topic. Finally, we suggest integrating large language models to enhance the flexibility of the fuzzy control systems, facilitating more dynamic and context-sensitive decision-making in managing pandemics.

Data availability statement

All data to reproduce the results of this research are provided in the manuscript.

Disclosure statement

The authors declare that there are no conflicts of interest.

Ethical statement

This study involves no human or animal subjects and uses only synthetic data for simulations, eliminating ethical concerns. No ethical approval or consent was required.

References

[1] Z. Abbasi, M. Shafieirad, A. H. Amiri Mehra, I. Zamani, *Optimized ANFIS-based control design using genetic algorithm to obtain the vaccination and isolation rates for the COVID-19*, in 2021 29th Iranian Conference on Electrical Engineering, ICEE 2021, IEEE, (2021), 731-735. https://doi.org/10.1109/ICEE52715.2021.9544298

[2] A. Adhikary, M. Pal, R. Maiti, *Impact of COVID-19 vaccinations in India: A state-wise analysis*, BMC Public Health, **25**(1) (2025), 219. https://doi.org/10.1186/s12889-025-21401-7

[3] C. Anastassopoulou, L. Russo, A. Tsakris, C. Siettos, *Data-based analysis, modelling and forecasting of the COVID-19 outbreak*, PLoS One, **15**(3) (2020), e0230405. https://doi.org/10.1371/journal.pone.0230405

[4] R. Arghal, S. S. Bidokhti, S. Sarkar, *Optimal capacity-constrained COVID-19 vaccination for heterogeneous populations*, Proceedings of the IEEE Conference on Decision and Control, (2022), 5620-5626. https://doi.org/10.1109/CDC51059.2022.9992682

[5] E. Badfar, E. J. Zaferani, A. Nikoofard, *Design a robust sliding mode controller based on the state and parameter estimation for the nonlinear epidemiological model of Covid-19*, Nonlinear Dynamics, **109**(1) (2022), 5-18. https://doi.org/10.1007/s11071-021-07036-4

[6] C. A. Bojan-Dragos, R. E. Precup, E. M. Petriu, R. C. Roman, E. L. Hedrea, A. I. Szedlak-Stinean, *GWO-based optimal tuning of controllers for shape memory alloy wire actuators*, IFAC-PapersOnLine, **55**(15) (2022), 39-44. https://doi.org/10.1016/j.ifacol.2022.07.605

[7] M. Borah, B. K. Roy, T. Kapitaniak, K. Rajagopal, C. Volos, *A revisit to the past plague epidemic (India) versus the present COVID-19 pandemic: Fractional-order chaotic models and fuzzy logic control*, European Physical Journal: Special Topics, **231**(5) (2022), 905-919. https://doi.org/10.1140/epjs/s11734-021-00335-2

[8] A. Buelta, A. Olivares, E. Staffetti, *Chance-constrained stochastic optimal control of epidemic models: A fourth moment method-based reformulation*, Computers in Biology and Medicine, **183** (2024), 109283. https://doi.org/10.1016/j.compbiomed.2024.109283

[9] B. Cao, T. Kang, *Nonlinear adaptive control of COVID-19 with media campaigns and treatment*, Biochemical and Biophysical Research Communications, **555** (2021), 202-209. https://doi.org/10.1016/j.bbrc.2020.12.105

[10] Z. Chen, L. Feng, H. A. Lay, K. Furati, A. Khaliq, *SEIR model with unreported infected population and dynamic parameters for the spread of COVID-19*, Mathematics and Computers in Simulation, **198** (2022), 31-46. https://doi.org/10.1016/j.matcom.2022.02.025

[11] X. Chen, C. Xiang, Y. Yang, *Sliding mode control of the susceptible-exposed-asymptomatic-infected-recovered model with vaccination*, Mathematical Methods in the Applied Sciences, **48**(3) (2025), 3936-3955. https://doi.org/10.1002/mma.10526

[12] C. Cheng, E. Aruchunan, M. H. Noor Aziz, *Leveraging dynamics informed neural networks for predictive modeling of COVID-19 spread: A hybrid SEIRV-DNNs approach*, Scientific Reports, **15**(1) (2025), 2043. https://doi.org/10.1038/s41598-025-85440-1

[13] B. Chhetri, V. M. Bhagat, S. Muthusamy, D. K. K. Vamsi, C. B. Sanjeevi, *Time optimal control studies on COVID-19 incorporating adverse events of the antiviral drugs*, Computational and Mathematical Biophysics, **9**(1) (2021), 214-241. https://doi.org/10.1515/cmb-2020-0125

[14] G. Chowell, C. Viboud, X. Wang, S. M. Bertozzi, M. A. Miller, *Adaptive vaccination strategies to mitigate pandemic influenza: Mexico as a case study*, PLoS One, **4**(12) (2009), e8164. https://doi.org/10.1371/journal.pone.0008164

[15] M. Coccia, *The evolution of COVID-19 pandemic wave and optimal levels of vaccination to reduce negative effects in society*, Research Square, (2021). https://doi.org/10.21203/rs.3.rs-941879/v1

[16] M. Dashtbali, M. Mirzaie, *A compartmental model that predicts the effect of social distancing and vaccination on controlling COVID-19*, Scientific Reports, **11**(1) (2021), 1-11. https://doi.org/10.1038/s41598-021-86873-0

[17] D. Faranda, T. Alberti, *Modeling the second wave of COVID-19 infections in France and Italy via a stochastic SEIR model*, Chaos, **30**(11) (2020), 1-13. https://doi.org/10.1063/5.0015943

[18] M. A. Hadi, H. I. Ali, *Control of COVID-19 system using a novel nonlinear robust control algorithm*, Biomedical Signal Processing and Control, **64** (2021), 102317. https://doi.org/10.1016/j.bspc.2020.102317

[19] S. Han, J. Cai, J. Yang, J. Zhang, Q. Wu, W. Zheng, H. Shi, M. Ajelli, X. H. Zhou, H. Yu, *Time-varying optimization of COVID-19 vaccine prioritization in the context of limited vaccination capacity*, Nature Communications, **12**(1) (2021), 4673. https://doi.org/10.1038/s41467-021-24872-5

[20] R. Ikram, A. Khan, M. Zahri, A. Saeed, M. Yavuz, P. Kumam, *Extinction and stationary distribution of a stochastic COVID-19 epidemic model with time-delay*, Computers in Biology and Medicine, **141** (2022), 105115. https://doi.org/10.1016/j.compbiomed.2021.105115

[21] J. S. Jia, X. Lu, Y. Yuan, G. Xu, J. Jia, N. A. Christakis, *Population flow drives spatio-temporal distribution of COVID-19 in China*, Nature, **582**(7812) (2020), 389-394. https://doi.org/10.1038/s41586-020-2284-y

[22] M. Khalighi, L. Lahti, F. Ndaïrou, P. Rashkov, D. F. Torres, *Fractional modelling of COVID-19 transmission incorporating asymptomatic and super-spreader individuals*, Mathematical Biosciences, **380** (2025), 109373. https://doi.org/10.1016/j.mbs.2024.109373

[23] K. K. F. Li, S. A. Jarvis, F. Minhas, *Elementary effects analysis of factors controlling COVID-19 infections in computational simulation reveals the importance of social distancing and mask usage*, Computers in Biology and Medicine, **134** (2021), 104369. https://doi.org/10.1016/j.compbiomed.2021.104369

[24] G. B. Libotte, F. S. Lobato, G. M. Platt, A. J. Silva Neto, *Determination of an optimal control strategy for vaccine administration in COVID-19 pandemic treatment*, Computer Methods and Programs in Biomedicine, **196** (2020), 105664. https://doi.org/10.1016/j.cmpb.2020.105664

[25] X. X. Liu, S. Hu, S. J. Fong, R. G. Crespo, E. Herrera-Viedma, *Modelling dynamics of coronavirus disease 2019 spread for pandemic forecasting based on Simulink*, Physical Biology, **18**(4) (2021), 1-20. https://doi.org/10.1088/1478-3975/abf990

[26] F. S. Lobato, G. B. Libotte, G. M. Platt, *Mathematical modelling of the second wave of COVID-19 infections using deterministic and stochastic SIDR models*, Nonlinear Dynamics, **106**(2) (2021), 1359-1373. https://doi.org/10.1007/s11071-021-06680-0

[27] A. H. A. Mehra, I. Zamani, Z. Abbasi, A. Ibeas, *Observer-based adaptive PI sliding mode control of developed uncertain SEIAR influenza epidemic model considering dynamic population*, Journal of Theoretical Biology, **482** (2019), 109984. https://doi.org/10.1016/j.jtbi.2019.08.015

[28] J. M. Mendel, *Type 2 fuzzy sets and systems: An overview*, IEEE Computational Intelligence Magazine, **2**(1) (2007), 20-29. https://doi.org/10.1109/MCI.2007.380672

[29] M. R. Mohammadi, M. Pourgholi, M. Nouri Manzar, *A fuzzy driver assistance system design with active disturbance rejection in autonomous vehicles with longitudinal movement*, Iranian Journal of Fuzzy Systems, **22**(1) (2025), 93-110. https://doi.org/10.22111/ijfs.2025.48966.8628

[30] B. Naffeti, Z. Ounissi, A. K. Srivastav, N. Stollenwerk, J. B. Van-Dierdonck, M. Aguiar, *Modeling COVID-19 dynamics in the Basque Country: Characterizing population immunity profile from 2020 to 2022*, BMC Infectious Diseases, **25**(1) (2025), 9. https://doi.org/10.1186/s12879-024-10342-y

[31] D. Niño-Torres, A. Ríos-Gutiérrez, V. Arunachalam, C. Ohajunwa, P. Seshaiyer, *Stochastic modeling, analysis, and simulation of the COVID-19 pandemic with explicit behavioral changes in Bogotá: A case study*, Infectious Disease Modelling, **7**(1) (2022), 199-211. https://doi.org/10.1016/j.idm.2021.12.008

[32] A. Olivares, E. Staffetti, *Optimal control-based vaccination and testing strategies for COVID-19*, Computer Methods and Programs in Biomedicine, **211** (2021), 106411. https://doi.org/10.1016/j.cmpb.2021.106411

[33] Y. Ouyang, S. Zhang, J. Xu, *A deterministic SAIR model with vaccination and treatment: Dynamical behaviors and control strategies*, Journal of Applied Mathematics and Computing, **71**(1) (2025), 573-604. https://doi.org/10.1007/s12190-024-02238-6

[34] R. E. Precup, R. C. Roman, E. L. Hedrea, A. I. Szedlak-Stinean, I. A. Zamfirache, *Classical and modern optimization techniques applied to control and modeling*, CRC Press, Taylor and Francis Group, (2025). https://doi.org/10.1201/9781003488279

[35] H. A. Rad, A. Badi, *A study on control of novel corona-virus (2019- nCoV) disease process by using PID controller*, MedRxiv, (2020), 1-9. https://doi.org/10.1101/2020.04.19.20071654

[36] H. Rafiei, M. R. Akbarzadeh-T, *Reliable fuzzy neural networks for systems identification and control*, IEEE Transactions on Fuzzy Systems, **31**(7) (2022), 2251-2263. https://doi.org/10.1109/TFUZZ.2022.3222036

[37] H. Rafiei, M. R. Akbarzadeh-T, *Hedge-embedded linguistic fuzzy neural networks for systems identification and control*, IEEE Transactions on Artificial Intelligence, **5**(10) (2024), 4928-4937. https://doi.org/10.1109/TAI.2024.3395416

[38] H. Rafiei, A. Salehi, F. Baghbani, P. Parsa, M. R. Akbarzadeh-T, *Interval type-2 fuzzy control and stochastic modeling of COVID-19 spread based on vaccination and social distancing rates*, Computer Methods and Programs in Biomedicine, **232** (2023), 107443. https://doi.org/10.1016/j.cmpb.2023.107443

[39] T. C. Reluga, *Game theory of social distancing in response to an epidemic*, PLoS Computational Biology, **6**(5) (2010), e1000793. https://doi.org/10.1371/journal.pcbi.1000793

[40] F. Rezaee-Ahmadi, H. Rafiei, M. R. Akbarzadeh-T, *Z-adaptive fuzzy inference systems*, in IEEE International Conference on Fuzzy Systems, Institute of Electrical and Electronics Engineers Inc., (2021). https://doi.org/10.1109/FUZZ45933.2021.9494413

[41] R. C. Roman, R. E. Precup, E. M. Petriu, A. I. Borlea, *Hybrid data-driven active disturbance rejection sliding mode control with tower crane systems validation*, Romanian Journal of Information Science and Technology, **27**(1) (2024), 50-64. https://doi.org/10.59277/ROMJIST.2024.1.04

[42] S. Saha, G. Samanta, J. J. Nieto, *Impact of optimal vaccination and social distancing on COVID-19 pandemic*, Mathematics and Computers in Simulation, **200** (2022), 285-314. https://doi.org/10.1016/j.matcom.2022.04.025

[43] P. Scarabaggio, R. Carli, G. Cavone, N. Epicoco, M. Dotoli, *Non-pharmaceutical stochastic optimal control strategies to mitigate the COVID-19 spread*, IEEE Transactions on Automation Science and Engineering, **19**(2) (2021), 560-575. https://doi.org/10.1109/TASE.2021.3111338

[44] S. Singh Negi, Ravina, N. Sharma, A. Priyadarshi, *Optimal control analysis on the spread of COVID-19: Impact of contact transmission and environmental contamination*, Gene, **941** (2025), 149033. https://doi.org/10.1016/j.gene.2024.149033

[45] A. Tarafdar, J. Mahato, R. K. Upadhyay, P. Bhattacharya, *Exploring the synergy of media awareness and quarantine classes in SiSAQEIHR model for pandemic control: A deep LSTM-RNN predictions*, Physica D, **474** (2025), 134563. https://doi.org/10.1016/j.physd.2025.134563

[46] J. Torres-Jiménez, Juan Pavón, *Applications of metaheuristics in real-life problems*, Progress in Artificial Intelligence, **2**(4) (2014), 175-176. https://doi.org/10.1007/s13748-014-0051-8

[47] C. Treesatayapun, *Epidemic model dynamics and fuzzy neural-network optimal control with impulsive traveling and migrating: Case study of COVID-19 vaccination*, Biomedical Signal Processing and Control, **71** (2022), 103227. https://doi.org/10.1016/j.bspc.2021.103227

[48] P. Yarsky, *Using a genetic algorithm to fit parameters of a COVID-19 SEIR model for US states*, Mathematics and Computers in Simulation, **185** (2021), 687-695. https://doi.org/10.1016/j.matcom.2021.01.022

[49] C. Zachreson, R. Tobin, C. Walker, E. Conway, F. M. Shearer, J. McVernon, N. Geard, *A model-based assessment of social isolation practices for COVID-19 outbreak response in residential care facilities*, BMC Infectious Diseases, **24**(1) (2024), 880. https://doi.org/10.1186/s12879-024-09788-x

[50] G. Zhang, Z. Li, A. Din, T. Chen, *Dynamic analysis and optimal control of a stochastic COVID-19 model*, Mathematics and Computers in Simulation, **215** (2024), 498-517. https://doi.org/10.1016/j.matcom.2023.08.005

APPENDIX I: PID CONTROLLER DESIGN

Furthermore, we examine the feasibility of a PID controller, optimized also by a genetic algorithm, under various scenarios. Here, two parallel, separate controllers are used as follows:

$$\begin{aligned} \upsilon[k] &= [P_{c1}, I_{c1}, D_{c1}][e[k], e[k]+e[k-1], \Delta e[k]]^T, \\ i[k] &= [P_{c2}, I_{c2}, D_{c2}][e[k], e[k]+e[k-1], \Delta e[k]]^T, \end{aligned} \tag{A.1}$$

where $P_{c1}, I_{c1}, D_{c1}, P_{c2}, I_{c1}, D_{c1}$ are parameters of two disjoint controllers. Also, $e[k]$ and $\Delta e[k]$ with $e[k] = (I_d[k] - \tilde{I}[k])/N[k]$ and $I_d[k]$ as the desired infected population at time k, which assumed to be zero in this study. The vaccination and isolation rates are then calculated using Eq. 10.

Tables 2-5 present M_1-M_3 for the PID controller. Also, Figures A.1-A.4 show the results of the PID controller for Scenarios 1-4, respectively. The designed PID controller lowers the infected population by consuming higher vaccination administrations than the proposed method. For instance, as Figure A.3 illustrates, the PID controller consumes all the vaccination capacity on the first day of the pandemic to reduce I.

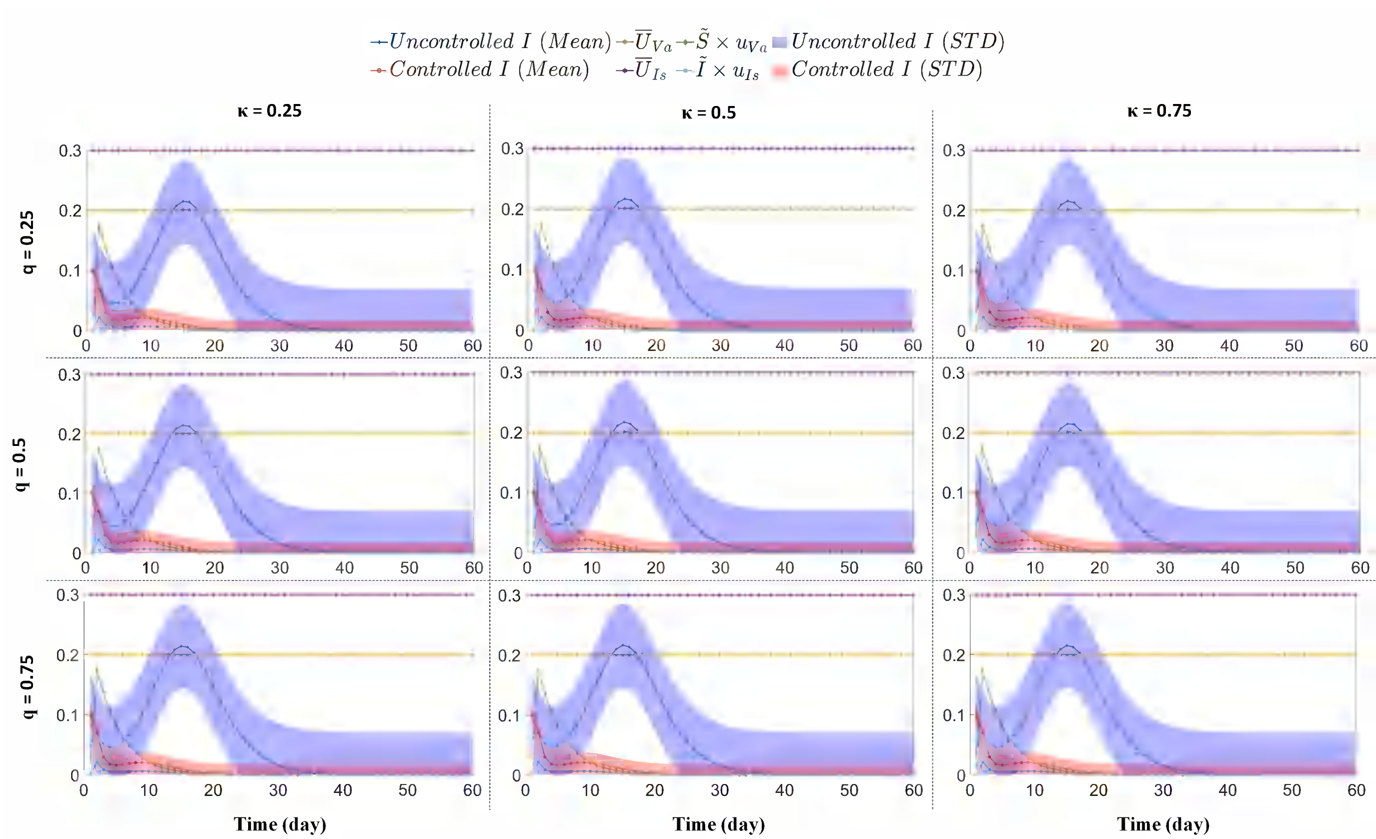

Figure A.1: Simulation results of Scenario 1 for various q and κ settings over sixty days for the PID controller.

APPENDIX II: TYPE-1 FUZZY CONTROLLER DESIGN

For comparative purposes, a type-1 fuzzy controller is designed here similarly to the proposed type-2 fuzzy controller, and its performance is evaluated.

The inputs to the fuzzy controller are the infected population ($I[k]$) and the upper bounds of vaccination and isolation ($\overline{U}_{Va}$ and $\overline{U}_{Is}$, respectively). The outputs of the fuzzy controller ($\upsilon[k]$ and $i[k]$) determine the appropriate fraction of vaccination and isolation to be applied at time k. Therefore, the type-1 fuzzy rules are as follows:

$$\text{If } I[k] \text{ is } A_1^l \text{ and } \overline{U}_{Va}[k] \text{ is } A_2^l \text{ and } \overline{U}_{Is}[k] \text{ is } A_3^l, \text{ then } \upsilon[k] \text{ is } B_1^l \text{ and } i[k] \text{ is } B_2^l, \tag{A.2}$$

where A_1^l, A_2^l, and A_3^l denote the type-1 fuzzy sets of the antecedent part and B_1^l and B_2^l are the fuzzy sets of the consequent of the l^{th} fuzzy rule with $l = 1, \ldots, M$.

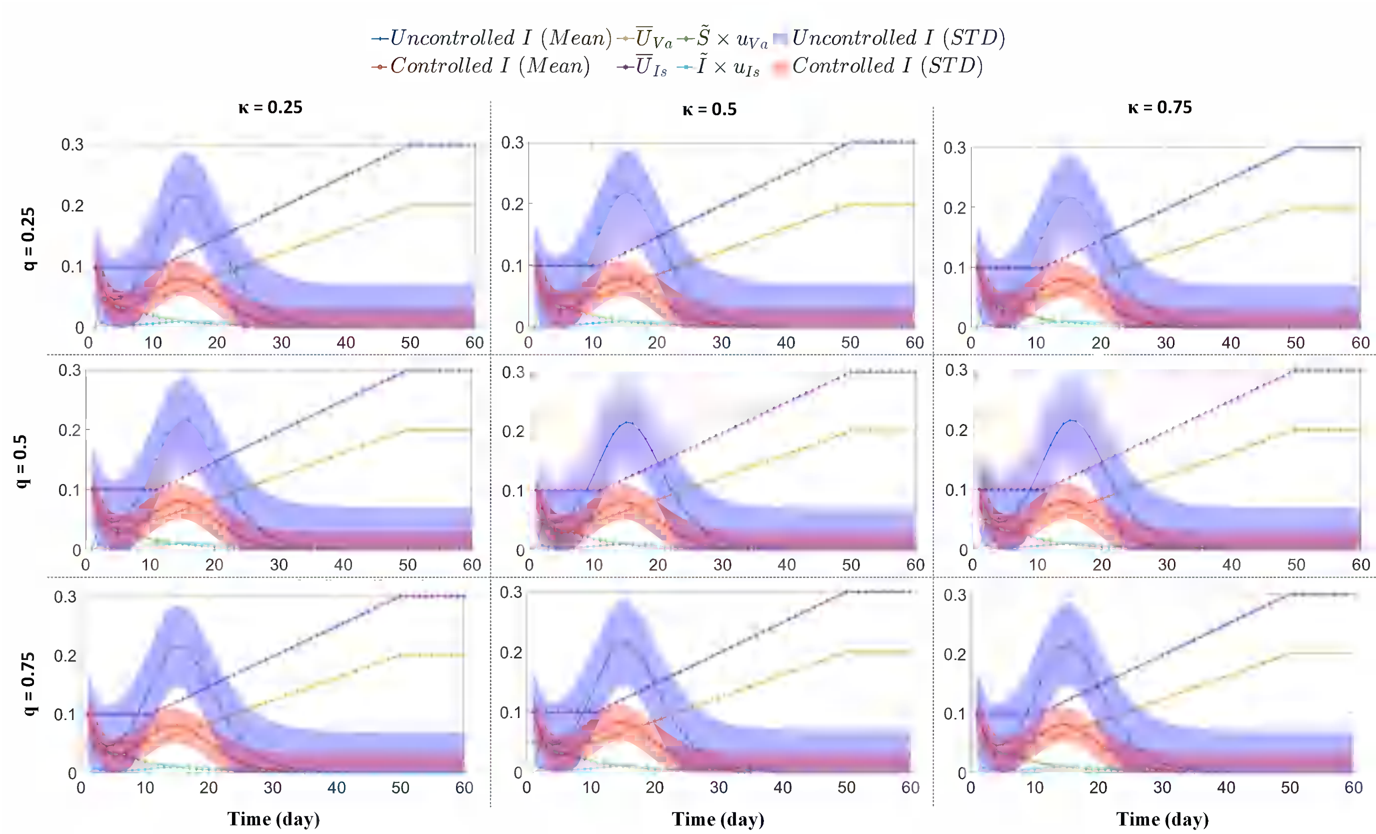

Figure A.2: Simulation results of Scenario 2 for various q and κ settings over sixty days for the PID controller.

The fuzzy controller uses a singleton fuzzifier, product inference engine, and centroid defuzzifier. The output is attained as follows:

$$[\upsilon[k], i[k]]^T = \frac{\sum_{l=1}^{L} \overline{W} f^l}{\sum_{l=1}^{L} f^l} = W^T \phi. \tag{A.3}$$

The vaccination and isolation rates are then calculated using Eq. 10.

Scenario 1 – with constant instant isolation and constraint

The fuzzy surfaces of the type-1 fuzzy controller are depicted in Figure A.5. As can be seen, the infected population (I) directly affects v and almost does not affect i. Also, $\overline{U}_{Va}$ does not affect υ while the increase of $\overline{U}_{Is}$ suggests a smaller i. Overall, the output of the fuzzy system does not have significant changes with the changes in its inputs. The infected population (controlled and uncontrolled), the vaccination and isolation cases ($\tilde{S}[k]u_{Va}$ and $\tilde{I}[k]u_{Is}$, respectively), and the upper bounds for isolation and vaccination rates ($\overline{U}_{Va}$ and $\overline{U}_{Is}$, respectively) are depicted in Figure A.6. The number of infected individuals has decreased significantly because of higher vaccination and isolation resources. Table 2 shows that the controller has reached its lowest number of infected individuals (M_1) compared to its remaining scenarios by applying higher vaccination administrations (M_2).

Scenario 2 - with time-varying instant isolation and vaccination constraint

For this scenario, the fuzzy surfaces are illustrated in Figure A.7. As illustrated, the fuzzy system suggests a higher υ with the rise of the vaccination upper bound. On the other hand, i is not much affected by the isolation upper bound ($\overline{U}_{Is}$). The infected population I affects i indirectly for $I < 0.5$ and indirectly for $I > 0.5$. Note that the fuzzy system output is almost constant for i according to the third axis. Also, the infected population, daily cases of vaccination and isolation, and $\overline{U}_{Va}$ and $\overline{U}_{Is}$ are illustrated in Figure A.8. As is depicted, the vaccines are administered in the early days, and the isolation cases are suggested during the disease peak. Table 3 shows that a higher M_1 is achieved compared to Scenario 1 because of tighter resource allocation to vaccination and isolation. In this scenario, M_3 is higher

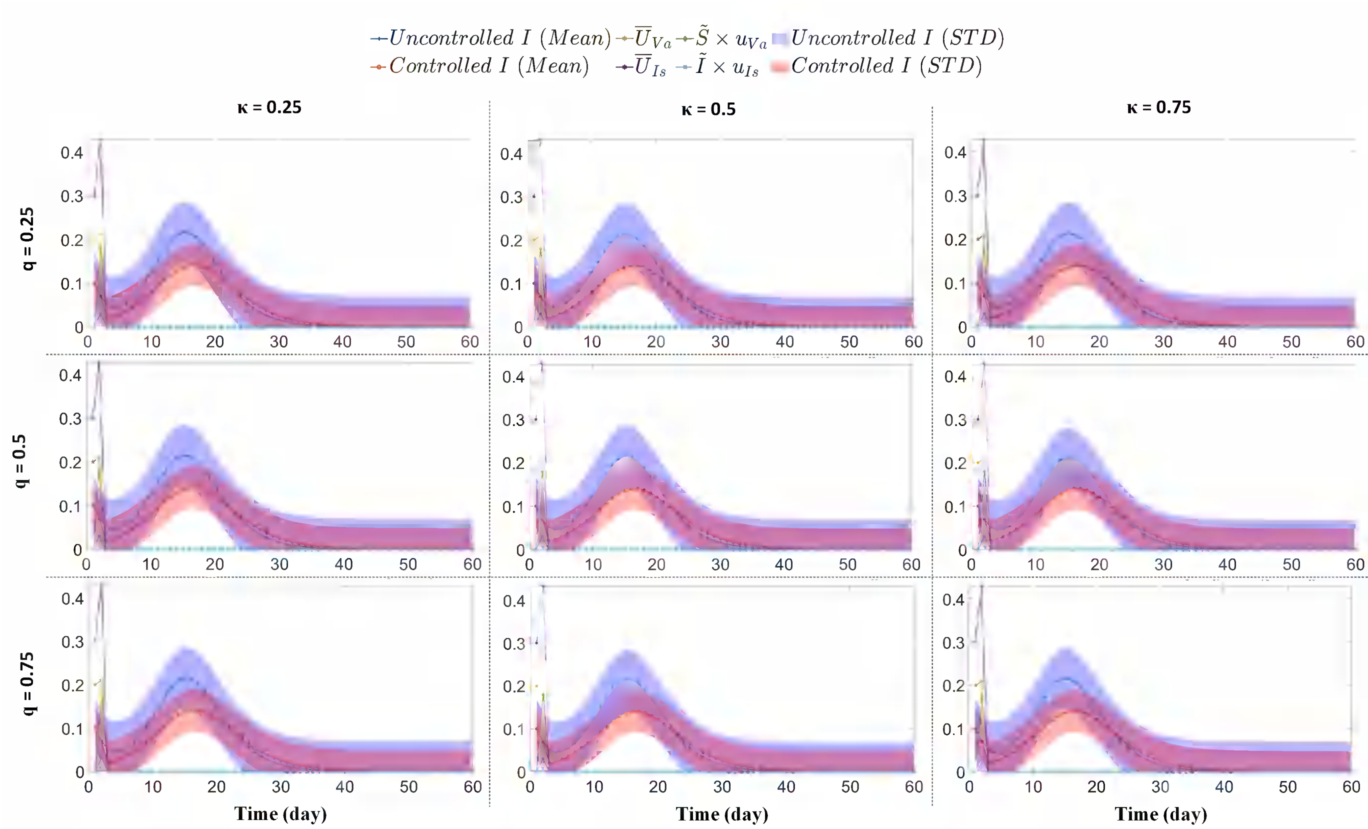

Figure A.3: Simulation results of Scenario 3 for various q and κ settings over sixty days for the PID controller.

than in Scenario 1. The tighter limitations on vaccination have caused the controller to reduce the number of infected individuals by higher isolation cases.

Scenario 3 - with constrained total number of vaccines and isolation

The fuzzy surfaces for Scenario 3 are depicted in Figure A.9 for the type-1 fuzzy controller. The fuzzy surfaces depict a direct relationship between the fuzzy outputs and the isolation and vaccination upper bounds. The isolation fraction (ι) is directly related to the infected population (I), while the rise in I results in a slight decrease of υ. The fuzzy output values on the third axis show that there is not much deviation in the outputs of the type-1 fuzzy system, and it almost suggests a constant value for all the variations of the fuzzy inputs. Also, the infected population (controlled and uncontrolled), the daily vaccination and isolation cases, and the upper bounds for isolation and vaccination rates are depicted in Figure A.10. As illustrated, all the limited resources are consumed in the first days to control the disease spread and reduce the infected population. According to Table 4, M_1 is higher than the two previous scenarios because the resource limitations are tighter. This conclusion can be observed from the lower M_2 and M_3 compared with the earlier scenarios.

Scenario 4 - with time-varying instant/cumulative isolation and vaccination constraint

For the fourth scenario, the fuzzy surfaces are depicted in Figure A.11. As can be seen, the rise of the infected population (I) increases ι, while it has almost an inverse effect on υ. The vaccination and isolation fractions (υ and ι, respectively) are inversely related upper own bounds ($\overline{U}_{Va}$ and $\overline{U}_{Is}$, respectively). The values of the third dimension demonstrate that, similar to the previous scenarios, the fuzzy system suggests almost a constant value and does not suggest an interpretable output. This result contrasts the type-2 fuzzy system, which depicts more dynamics in selecting appropriate outputs. The infected population, the rates' upper bounds, and the isolation and vaccination cases are illustrated in Figure A.12. Similar to the type-2 fuzzy system, the available vaccination and isolation resources are expended in the first days of disease spread to reduce the infected population. According to Table 5, $M_1 - M_3$ are similar to Scenario 3, because of similar resource limitations.

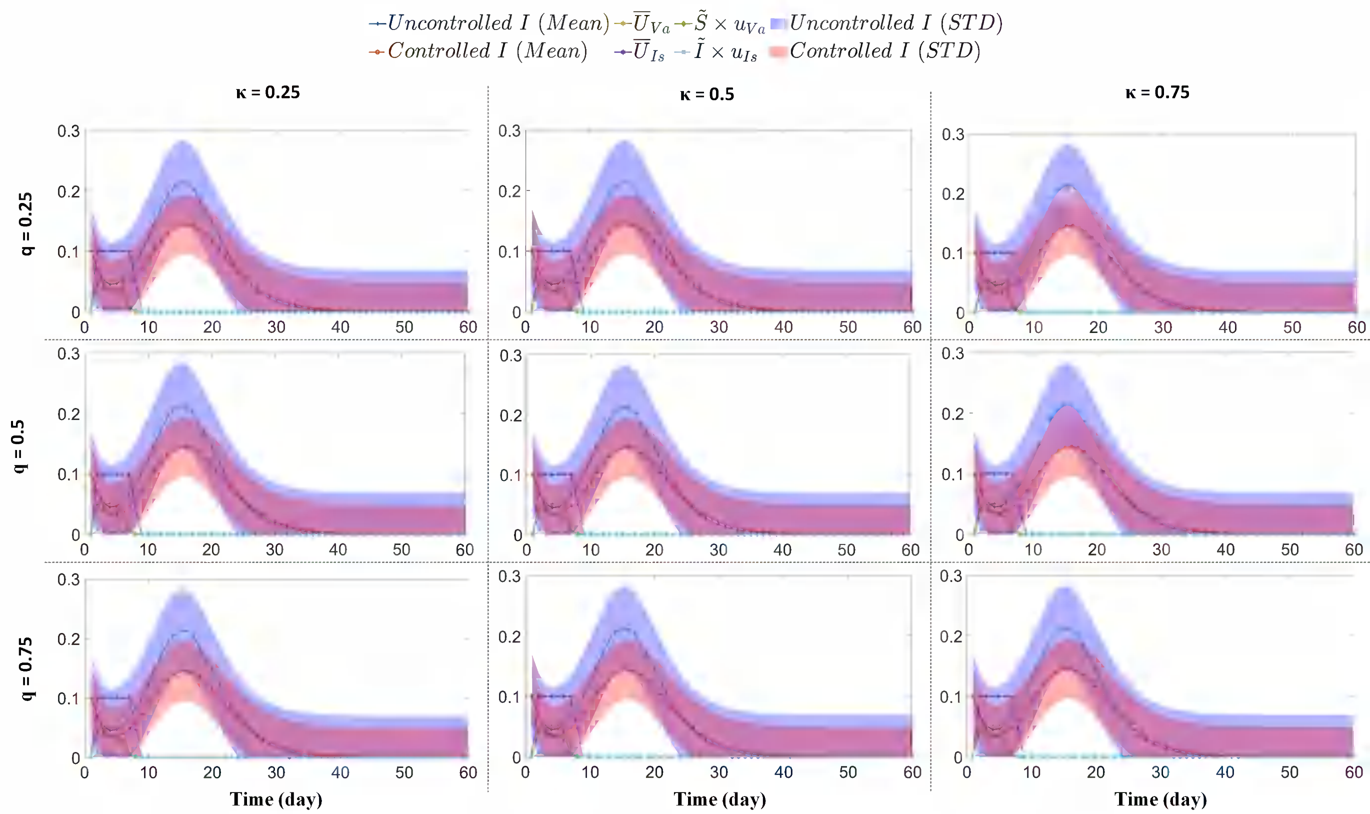

Figure A.4: Simulation results of Scenario 4 for various q and κ settings over sixty days for the PID controller.

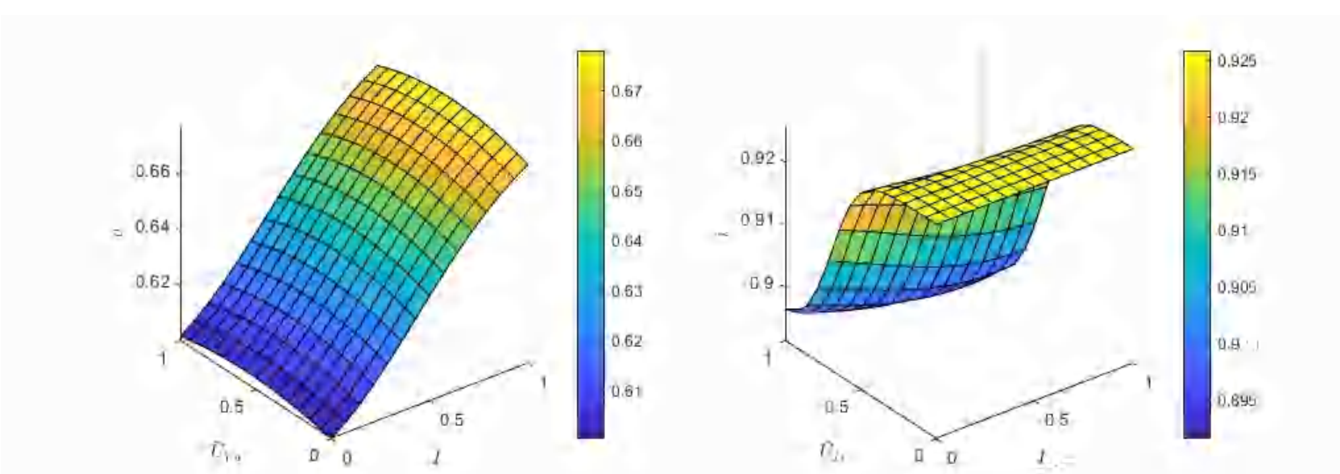

Figure A.5: The fuzzy surface of the type-1 fuzzy controller for Scenario 1: left) the fuzzy surface of v with respect to I and $\overline{U}_{Va}$ right) the fuzzy surface of i with respect to I and $\overline{U}_{Is}$. The goal in the first scenario is to diminish the infected population in the presence of fixed daily upper bounds for vaccination and isolation.

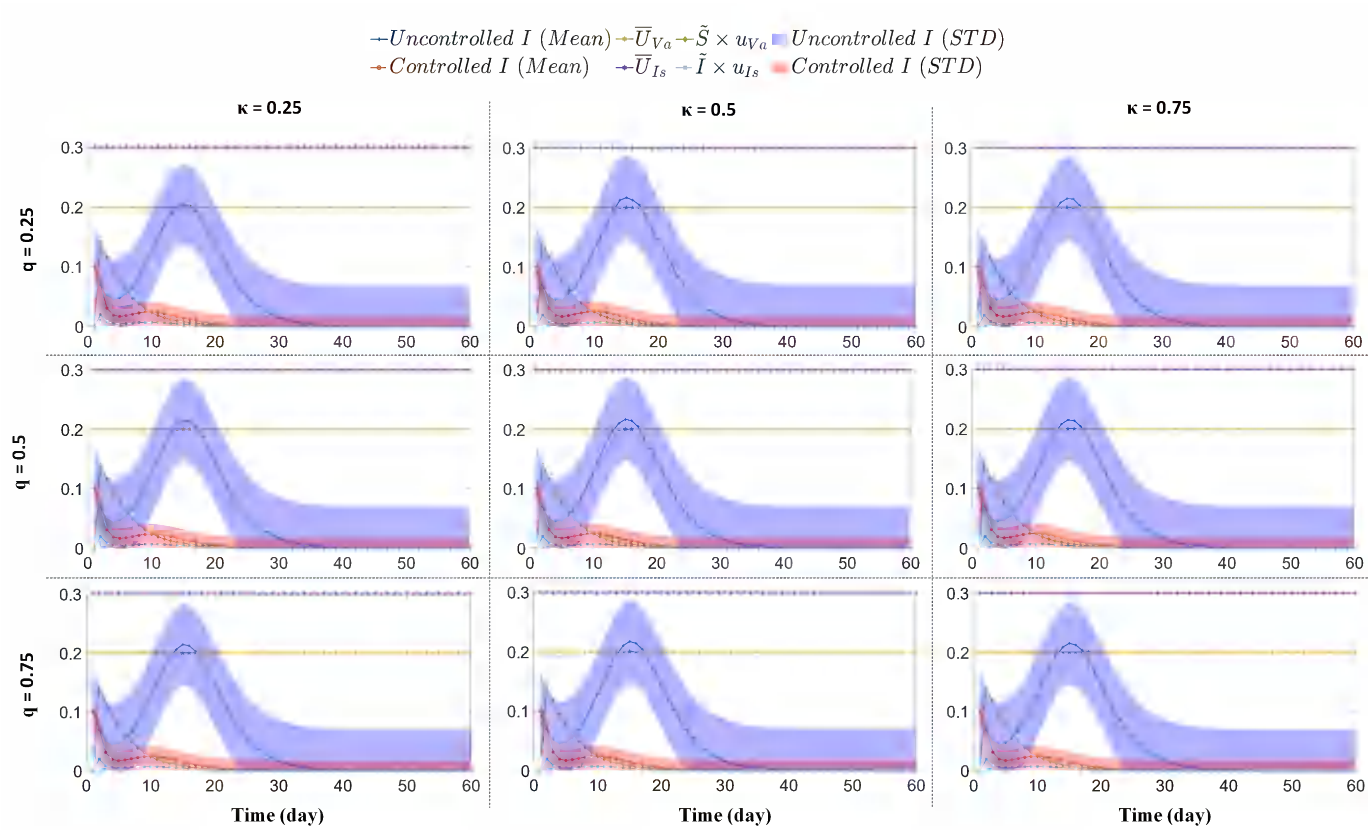

Figure A.6: Comparing the infected population size (controlled, desired, and uncontrolled), vaccination rate, and isolation rate over sixty days with different q and κ in Scenario 1 for the type-1 fuzzy controller.

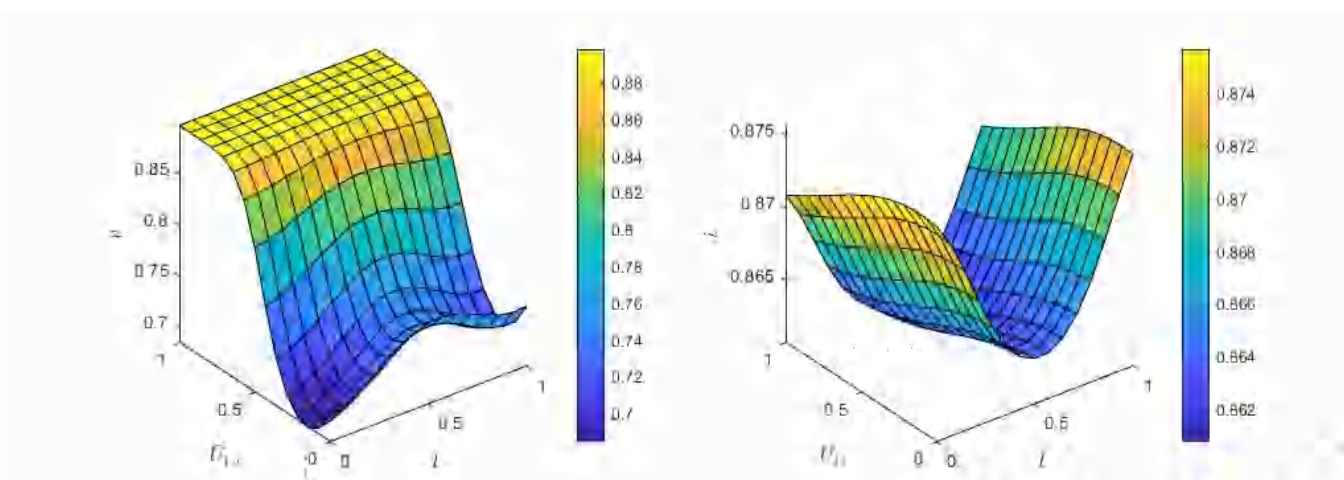

Figure A.7: The fuzzy surface of the type-1 fuzzy controller for Scenario 2: left) the fuzzy surface of v with respect to I and $\overline{U}_{Va}$, right) the fuzzy surface of i with respect to I and $\overline{U}_{Is}$. The goal in the second scenario is to diminish the infected population in the presence of time-varying daily upper bounds for vaccination and isolation.

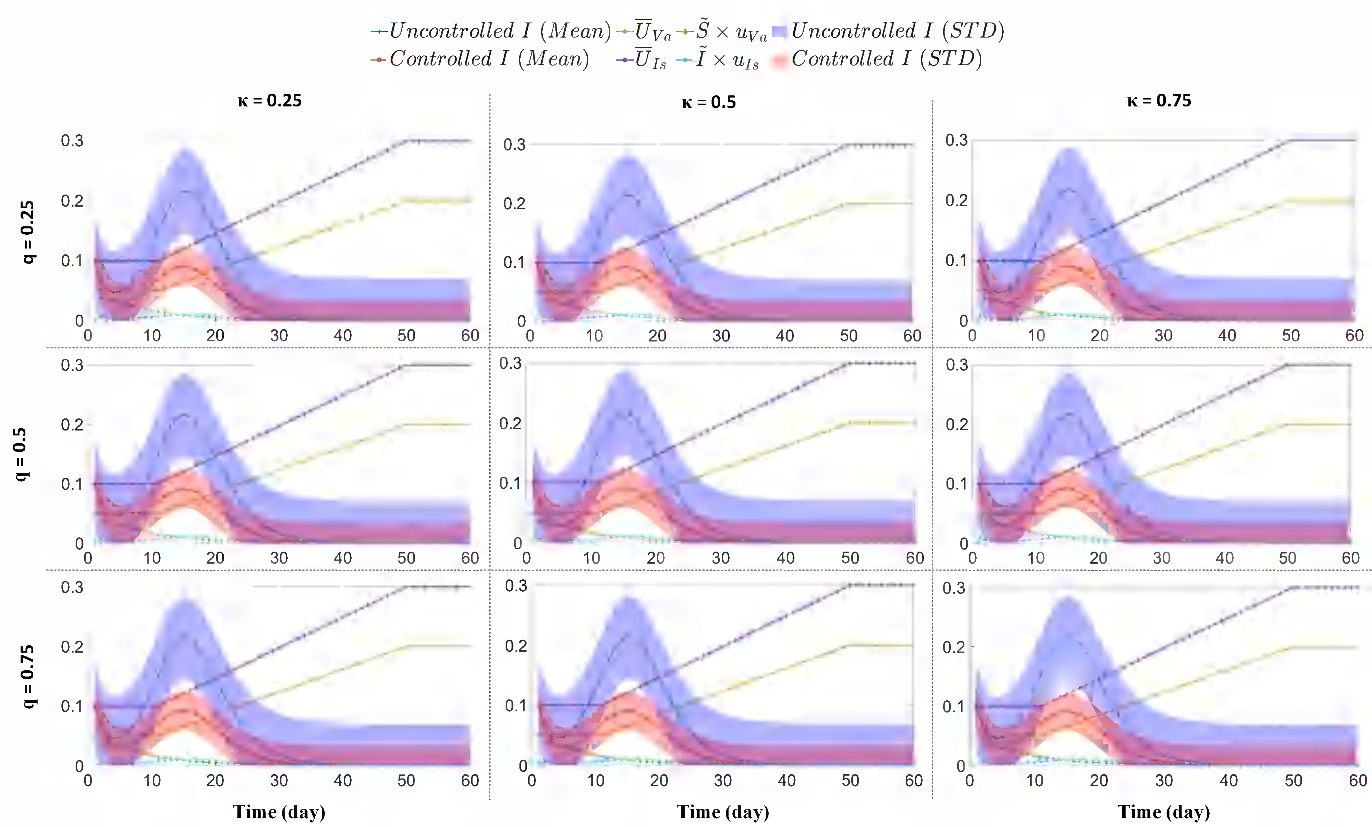

Figure A.8: Simulation results of Scenario 2 for various values of q and κ over sixty days for the type-1 fuzzy controller.

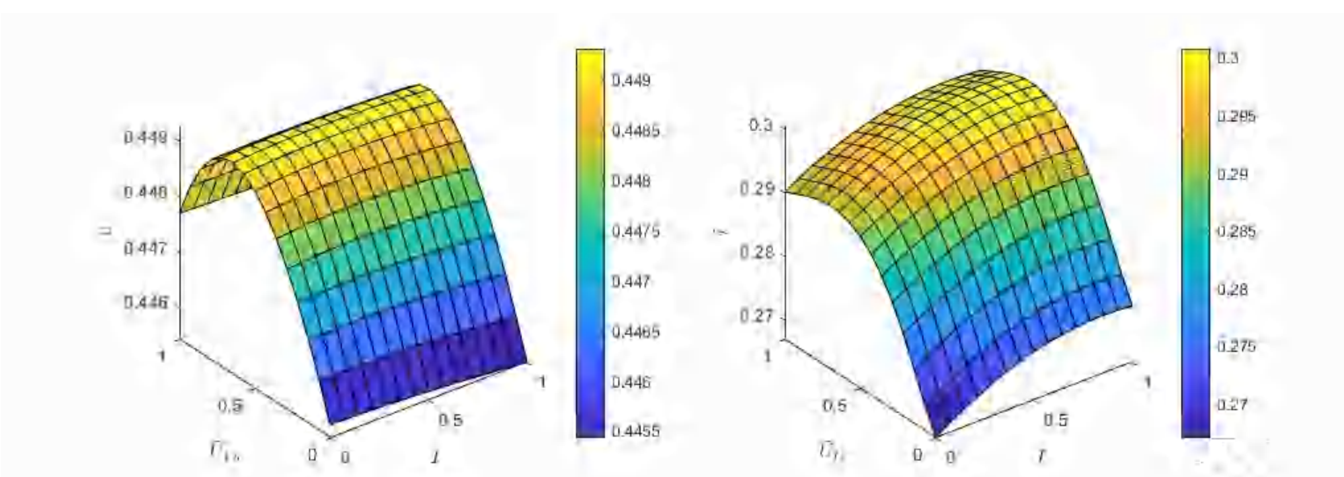

Figure A.9: The fuzzy surface of the type-1 fuzzy controller for Scenario 3: left) The fuzzy surface of v with respect to I and $\overline{U}_{Va}$ right) the fuzzy surface of i with respect to I and $\overline{U}_{Is}$. The goal in the third scenario is to diminish the infected population in the presence of limited supplies for vaccination and isolation.

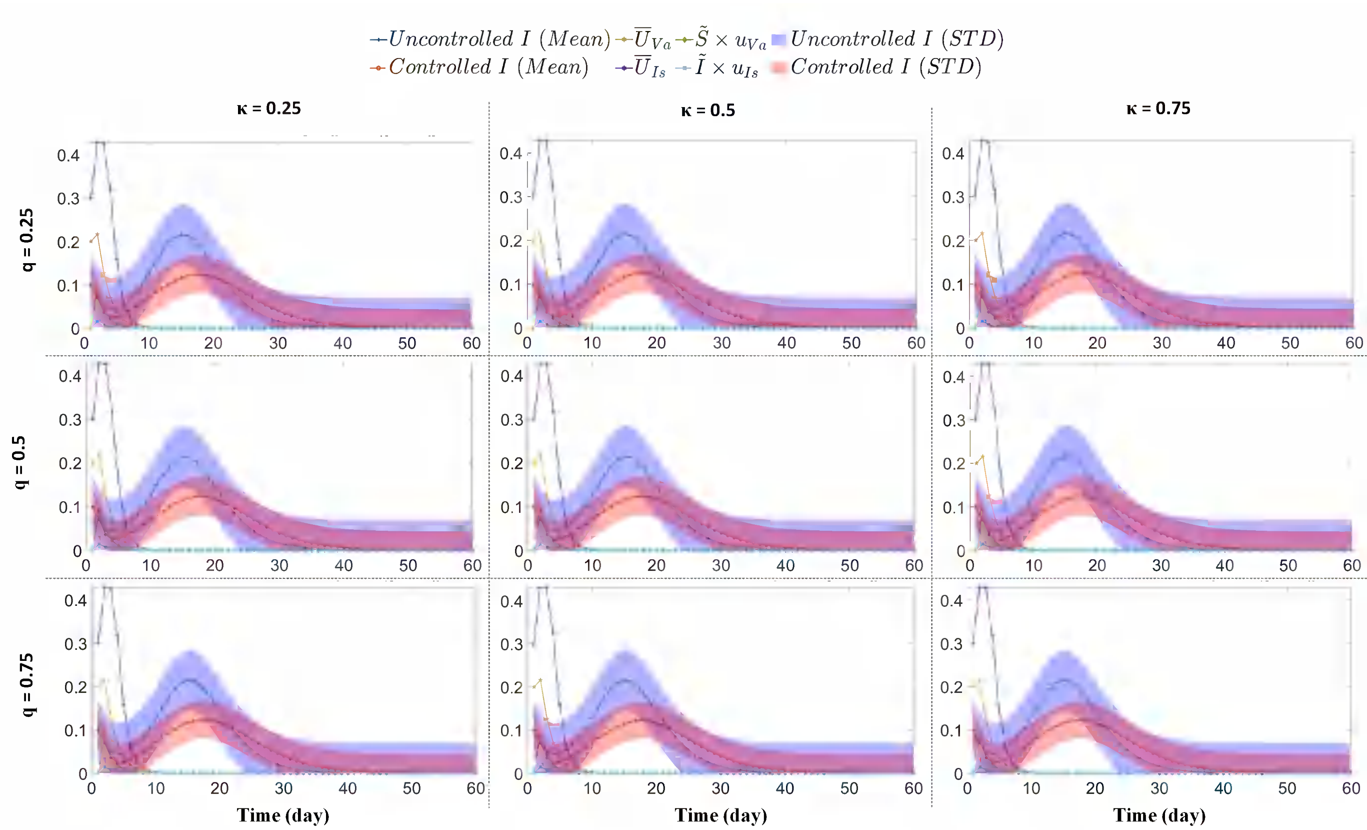

Figure A.10: Simulation results of Scenario 3 for various values of q and κ over sixty days for the type-1 fuzzy controller.

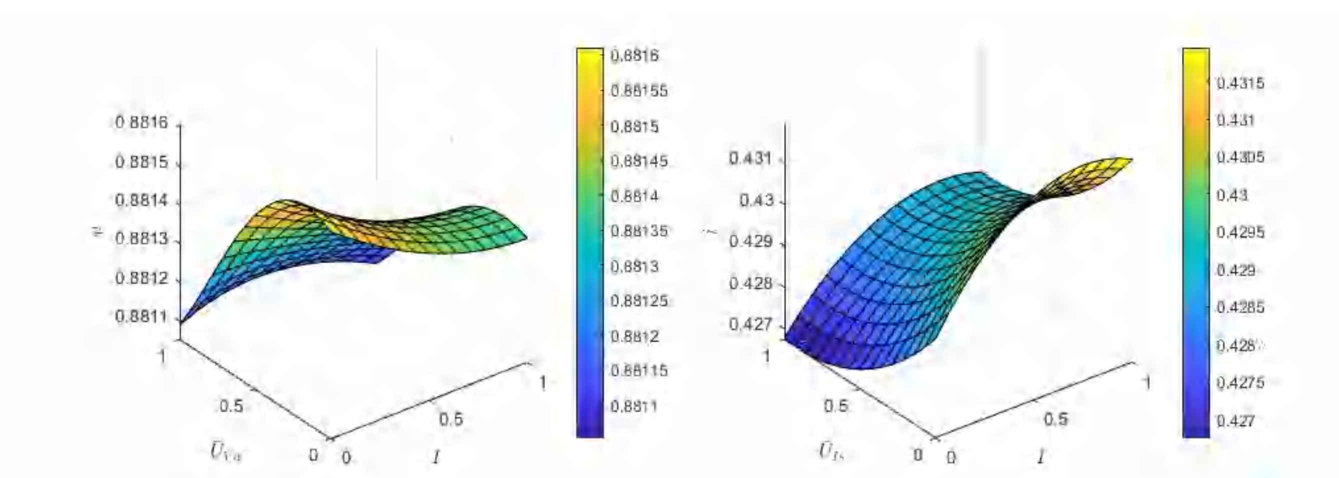

Figure A.11: The fuzzy surface of the type-1 fuzzy controller for Scenario 4: left) the fuzzy surface of υ concerning I and $\overline{U}_{Va}$ right) the fuzzy surface of i concerning I and $\overline{U}_{Is}$. The goal in the fourth scenario is to diminish the infected population in the presence of both limited supplies and time-varying daily upper bounds for vaccination and isolation rates.

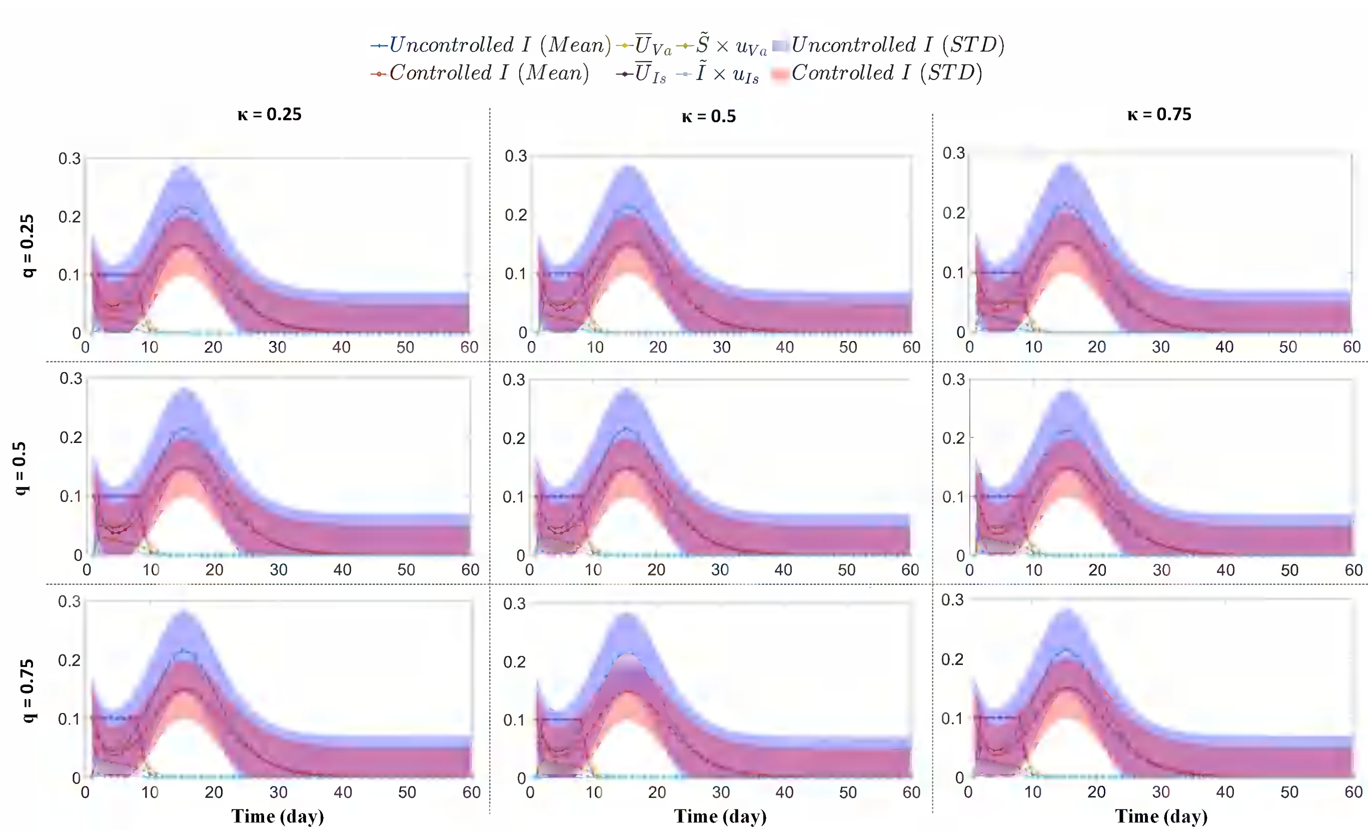

Figure A.12: Simulation results of Scenario 4 for various values of q and κ over sixty days for the type-1 fuzzy controller.